Stark ionization in dc and ac fields: An L^2 complex-coordinate approach

A. Maquet* and Shih-I Chu†
Joint Institute for Laboratory Astrophysics, University of Colorado and National Bureau of Standards, Boulder, Colorado 80309

William P. Reinhardt
Department of Chemistry, University of Colorado, Boulder, Colorado 80309 and Joint Institute for Laboratory Astrophysics, University of Colorado and National Bureau of Standards, Boulder, Colorado 80309

(Received 19 November 1982)

A finite-dimensional—matrix technique valid for computation of complex eigenvalues and eigenfunctions useful for discussing time evolution in both dc and ac Stark fields is presented. The complex eigenvalue parameters are those of appropriately analytically continued, time-independent Stark Hamiltonians as obtained via the complex scale transformation $r \rightarrow re^{i\theta}$. Such a transformation distorts the continuous spectrum away from the real axis, exposing the Stark resonances, and also allowing use of finite variational expansions employing L^2 basis functions chosen from a complete discrete basis. The structure of the dc and ac Stark Hamiltonians is discussed and extensive convergence studies performed in both the dc and ac cases to fully document the utility of the method. Sudden and adiabatic dc Stark time evolution is used to illustrate the power of finite-dimensional—matrix methods in describing complex, multiple-time-scale time evolution. The relationship between the ac Stark Hamiltonian used (a time-independent truncated Floquet Hamiltonian) and continued-fraction perturbation theory follows easily via use of matrix partitioning, and provides a particularly straightforward derivation of these results. Finally, some illustrative calculations of off-resonant generalized cross sections are given at low and high intensities, indicating that the method works satisfactorily at intensities the order of internal atomic field strengths. A more detailed discussion of time evolution in two-, three-, and four-photon ionization processes appears in the following paper by Holt, Raymer, and Reinhardt.

I. INTRODUCTION

Over the past several years the technique of continued-fraction perturbation theory has been the most used computational approach to the problem of atomic multiphoton ionization.[1] In this paper we give a detailed presentation[2] of an alternative finite-dimensional—matrix computational technique which has advantages in terms of simplicity of organization of computations, in terms of its ability to self-consistently treat intense field effects, (in that all atomic levels are simultaneously shifted and broadened by the external field), and in terms of the straightforward inclusion of free-free transitions and the effects of coupling between electronic continua. As the two major conceptualizations—use of complex coordinates, and L^2 discretization—which allow development of the technique are nonstandard in this area of application, a major purpose of this paper is the systematic exposition of the complex-valued—matrix technique.

We note that the use of a complete discrete L^2 basis obviates the necessity of explicit introduction of exact atomic bound and continuum states, thus reducing all computations to those involving finite-dimensional matrices.[3] Thus, in particular, use of finite-dimensional matrices does not imply neglect of continua.[3] The use of complex coordinates[4,5] not only allows direct calculation of eigenvalue parameters associated with complex dressed states, but completely avoids numerical problems arising from strong coupling between overlapping atomic continua.

Another major purpose of the present exposition is to provide the details of the connection between the complex-valued—matrix technique and continued-fraction expansion of resolvent matrix elements. Once these connections are established,

applications are appropriate. These appear in paper by Holt, Raymer, and Reinhardt (HRR),[6] where the time dependence of some two-, three-, and four-photon ionization processes in atomic H are considered.

In order to separate considerations of the use of complex coordinates and L^2 discretization from the multiphoton problem, we consider first the problem of dc Stark ionization. Discussion of the block matrix structure of the Stark Hamiltonian sets the stage for discussion of the analogous block structure of the corresponding ac Stark Hamiltonian (Floquet Hamiltonian). Earlier computational treatments of the dc problem using these techniques[7] are then extended in two ways: An extended convergence study is carried out, not only to demonstrate that results of very high precision can be obtained, but to give results of high enough precision to verify recent results of summation of the Rayleigh-Schrödinger perturbation series by the Padé[8] and Borel[9] methods. This is followed (Sec. II B) by a discussion of the detailed time evolution of field ionization of the H atom, placed suddenly or adiabatically in an intense dc field. This latter example of the use of complex coordinates and L^2 discretization demonstrates that it is possible, using finite-dimensional—matrix techniques, to construct time-evolution operators which yield converged results for quite complicated irreversible time dependences. Application to time dependences in multiphoton ionization appears in HRR.

Section III introduces the time-independent Floquet or Hamiltonian needed to extend the matrix technique to the ac case. The discussion is brief but explicit, as the form of the Hamiltonian introduced here underlies the analysis of Secs. IV and V. In Sec. IV the extension of the coordinate-space Floquet Hamiltonian to use of complex coordinates is made by analogy with the dc Stark case, and the optimal arrangement of the matrix block structure for matrix computations is discussed. Convergence of complex eigenvalues for representative ionization processes is demonstrated as a function of basis size, nonlinear parameters, and truncation of the Floquet block structure. The Appendix contains a brief outline of the computational algorithm used to extract individual complex eigenvalues from large complex Floquet matrices with good numerical efficiency. In particular, contact is made with the recent work of Wyatt *et al.*[10] The detailed relationship between the complex poles of the resolvent of the Floquet Hamiltonian and continued-fraction perturbation theory is given in Sec. V, where a direct derivation in terms of block-matrix algebra (matrix partitioning) is given. Connection is also made between various truncations of the matrix Floquet Hamiltonian and diagrammatic representations of the infinite-order perturbation summations implicit in extraction of eigenvalues of the Hamiltonian. In Sec. VI, to exemplify application of the method, results of calculations of the intensity and wavelength dependence for one- and two-photon-dominated processes are given in the limit where nonadiabatic effects may be reasonably neglected (i.e., not too close to resonance), and thus generalized cross sections defined. The more interesting case of resonant or near-resonant processes is discussed in HRR. Finally, a summary and discussion are given in Sec. VII.

II. THE dc PROBLEM: COMPLEX EIGENVALUES AND FIELD IONIZATION

The dc Stark problem occupies a central role in the study of perturbation theory in quantum mechanics. Low-order results give accurate atomic level shifts, yet the series diverges strongly in large order,[8,9,11] a result intimately connected with the fact that the Stark Hamiltonian (shown here for the H atom)

$$H^{\text{Stark}} = -\tfrac{1}{2}\nabla^2 - \frac{1}{r} - Fz \tag{2.1}$$

has no bound-state eigenvalues. As discussed first by Titchmarsh,[12] the poles of the unperturbed resolvent $(z - H^{\text{atom}})^{-1}$ where

$$H^{\text{atom}} = -\tfrac{1}{2}\nabla^2 - \frac{1}{r} \tag{2.2}$$

have been shifted onto a higher Riemann sheet on application of the "perturbation"—Fz. The divergent Rayleigh-Schrödinger perturbation expansion is thus interpreted as giving an asymptotic expansion for the real part of the complex poles of the resolvent. More recently the divergent expansion has been summed by the Borel[9] and Padé[8] techniques to very high accuracy, giving both the real *and imaginary* parts of the pole positions. One purpose of this section is to present converged variational results of sufficient precision to be able to confirm the summed perturbative results. The other is to establish the complex-coordinate matrix formalism, before introducing it in the context of multiphoton ionization. This latter is accomplished in Sec. II A, followed by a discussion of time dependence in sudden and adiabatic dc field ionization in Sec. II B.

A. Complex-coordinate matrix discretization and the dc Stark problem

Variational calculation of the real and imaginary parts of the poles of the analytically continued dc Stark resolvent clearly cannot begin with the Hamil-

tonian of Eq. (2.1): this Hamiltonian has no discrete eigenvalues, and its continuous spectrum is the whole real axis from $-\infty$ to $+\infty$.[12] However, as has been demonstrated numerically,[7] and subsequently justified as a rigorous result of functional analysis,[13] the dilated Hamiltonian ($z=r\cos\alpha$)

$$H^{\text{Stark}}(\theta)\equiv -\frac{e^{-2i\theta}}{2}\nabla^2-\frac{e^{-i\theta}}{r}-e^{i\theta}Fr\cos\alpha \tag{2.3}$$

obtained by the transformation to complex coordinates, $r\rightarrow re^{i\theta}$ (θ will be taken real) has complex eigenvalues, with corresponding square-integrable (L^2) eigenfunctions, corresponding to the poles of Hilbert-space matrix elements of the analytically continued resolvent. As the eigenfunctions are L^2 we can expect an appropriate expansion in L^2 basis functions to approximate them. Linear variational determination of approximate eigenvalues and eigenfunctions is entirely equivalent to finding the appropriate matrix eigenvalues and eigenvectors of the representation of $H^{\text{Stark}}(\theta)$ in the basis.

Working in usual spherical polar coordinates (r,α,φ), a complete set of basis functions for expansion of a nonspherically symmetric, but L^2, function is the set

$$\phi_{n,l,m_l}(r,\alpha,\varphi)=C_{n,l}(\lambda)r^{l+1}e^{-(\lambda/2)r}L_n^{2l+2}(\lambda r)\times Y_{l,m}(\alpha,\varphi)\ , \tag{2.4}$$

where

$$C_{n,l}(\lambda)r^{l+1}e^{-(\lambda r/2)}L_n^{2l+2}(\lambda r) \tag{2.5}$$

are the complete (but discrete) set of generalized orthonormal Laguerre-type radial functions, and the $Y_{l,m}(\alpha,\varphi)$ are the usual spherical harmonics. Matrix elements of the spherically symmetric atomic Hamiltonian are of the form

$$\langle n,l,m_l\,|\,H^{\text{atom}}(\theta)\,|\,n',l',m_{l'}\rangle=\int_0^\infty dr\int_0^\pi \sin\alpha\,d\alpha\int_0^{2\pi}d\varphi\,\phi^*_{n,l,m_l}(r,\alpha,\varphi)\left[-e^{-2i\theta}\frac{\nabla_1^2}{2}-\frac{e^{-i\theta}}{r}\right]\times\phi_{n',l',m_{l'}}(r,\alpha,\varphi) \tag{2.6a}$$

which factors as

$$C_{n,l}(\lambda)C_{n',l'}(\lambda)\int_0^\infty dr\,r^{l+1}e^{-\lambda r/2}L_n^{2l+2}(\lambda r)\left[-e^{-2i\theta}\frac{1}{2}\frac{d^2}{dr^2}-\frac{e^{-i\theta}}{r}\right]r^{l+1}e^{-\lambda r/2}L_n^{2l+2}(\lambda r)\delta_{l,l'}\delta_{m_l,m_{l'}} \tag{2.6b}$$

giving a block-diagonal structure labeled by the angular momentum l, where we denote in the usual spectroscopic notation as $s,p,d,\ldots$, for $l=0,1,2,\ldots$,etc. Each l block will be taken to have dimension N_l, determined by the number of radial basis functions kept in the expansion. The perturbation, $e^{i\theta}Fr\cos\alpha$, acts as a point dipole giving the usual $\Delta l=\pm1$ and $\Delta m_l=0$ selection rules:

$$\begin{aligned}&\langle n,l,m_l\,|\,e^{i\theta}Fr\cos\alpha\,|\,n',l',m_{l'}\rangle\\&=e^{i\theta}\left[C_{n,l}(\lambda)C_{n'l'}(\lambda)\int_0^\infty r^2dr\,r^le^{-\lambda r/2}L_n^{2l+2}(\lambda r)(Fr)r^{l'}e^{-\lambda r/2}\right.\\&\left.\times L_n^{2l'+2}(\lambda r)\int_0^\pi\sin\alpha\,d\alpha\int_0^{2\pi}d\varphi\,Y^*_{l,m_l}(\alpha,\varphi)\cos\alpha\,Y_{l'm_{l'}}(\alpha,\varphi)\right]\delta_{l\pm1,l'}\delta_{m_l,m_{l'}}\ .\end{aligned} \tag{2.6c}$$

The interaction with the field thus gives a tridiagonal block-matrix structure connecting consecutive diagonal blocks, to form the overall block tridiagonal structure indicated in Fig. 1. Computation of the variationally determined (complex for $\theta\neq0$) coefficients, a_{n,l,m_l} in the expansion of approximate L^2 eigenfunctions of $H^{\text{Stark}}(\theta)$ of the form

$$\psi(r,\alpha,\varphi)=\sum_{l=0}^{l_{\max}}\sum_{n=1}^{N_l}a_{n,l,m_l}\phi_{n,l,m_l}(r,\alpha,\varphi) \tag{2.7}$$

and corresponding (complex) approximate eigenvalues reduces to finding matrix eigenvalues and eigenvectors of the matrix defined by Eqs. (2.6), and shown schematically in Fig. 1. In Eq. (2.7), N_l indi-

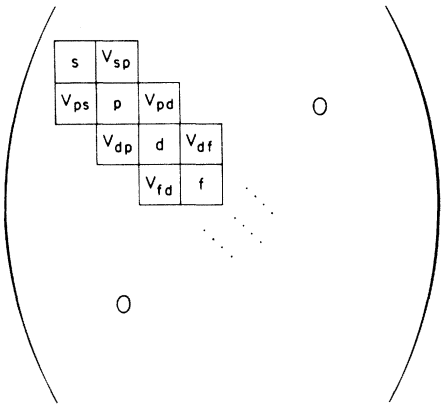

FIG. 1. Tridiagonal block-matrix structure of the dc Stark Hamiltonian in the spherically symmetric basis of Eq. (2.6). This structure is generalized (see Figs. 5 and 6) to treat the ac Stark effect in linear polarization.

cates the number of radial functions for a given l value, and $l_{\max}$ indicates the maximum l value kept in the summation. The azimuthal quantum number m_l is not summed over as both the atomic and perturbative Hamiltonians are diagonal in this quantum number. Finding the eigenvectors and eigenvalues of the matrix eigenvalue problem $\bar{H}^{\text{atom}}(\theta) + e^{i\theta}\overline{Fr}$ corresponds to a linear variation of the coefficients in Eq. (2.7), and is just the analytic continuation of the usual Rayleigh-Ritz linear variational theory.[4] We also note that as the *actual* eigenfunction $\psi(\theta)$ of the Stark Hamiltonian $H^{\text{Stark}}(\theta)$, is L^2, that the expansion basis of Eq. (2.4) should be, and is, perfectly adequate to the task.

Determination of these matrix eigenvalues is a standard problem in the numerical analysis of linear systems. Equations (2.6) contain the nonlinear scale parameters θ and λ. Thus, if the expansion of Eq. (2.7) is truncated, (i.e., if N_l and $l_{\max} \neq \infty$) the basis is incomplete, but will usually give an excellent approximation provided that (i) the truncated N_l and $l_{\max}$ are large enough and (ii) the nonlinear parameters λ and θ are appropriately chosen. Both points (i) and (ii) must be addressed by a combination of trial and error and physical intuition. It is the purpose of the remainder of this section to indicate how this can be done in a reasonable and systematic manner.

Focusing attention on the complex eigenvalue corresponding to the broadened and shifted $1s\ 1^2S$ state of atomic hydrogen, whose radial wave function (atomic units, $\hbar = m_e = e^2 = 1$, assumed) has the form e^{-r}, indicates that a plausible first estimate of

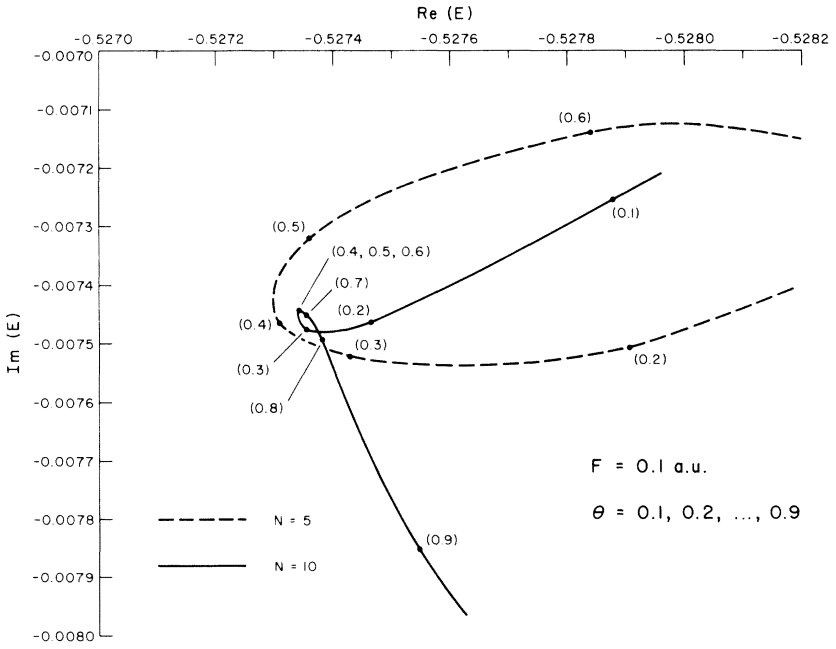

FIG. 2. Quasivariational determination of an optimal value of θ in the dc Stark case. Complex eigenvalue corresponding to the shifted and broadened $1s$ state of atomic hydrogen is calculated in a finite L^2 basis as a function of the rotation angle θ in the transformation $r \rightarrow re^{i\theta}$. For the case of ten basis functions (per atomic symmetry) a stationary point near $\theta = 0.4$ is found, indicating that this is a reasonable choice of θ for convergence studies (see Tables I and II). Figure reproduced from Ref. 7.

TABLE I. Convergence of $-\Gamma/2$ for the $1s$ state of hydrogen in a dc field of 0.1 a.u. ($\approx 5.6\times 10^8$ V/cm). Number of atomic symmetries is $l_{\max}+1$, and N denotes the number of Laguerre-type functions per atomic symmetry. Numbers in parentheses are exponents. Thus the results for $l_{\max}=10$ and $l_{\max}=11$ suggest a converged value $\Gamma/2=0.007\,269\,057$, with uncertainty ± 1 in the last figure. $\theta=0.4$ in all calculations (see text).

	$l_{\max}=8$		$l_{\max}=9$	$l_{\max}=10$	$l_{\max}=11$
N	$\lambda=1.5$	$\lambda=2.0$	$\lambda=2.0$	$\lambda=2.0$	$\lambda=2.0$
14	$-0.726\,916\,98(-2)$[a]	$-0.726\,916\,48(-2)$	$-0.726\,904\,36(-2)$	$-0.726\,904\,92(-2)$	
15	$-0.726\,916\,10(-2)$	$-0.726\,916\,49(-2)$	$-0.726\,904\,06(-2)$	$-0.726\,905\,81(-2)$	$-0.726\,905\,69(-2)$
16	$-0.726\,916\,41(-2)$	$-0.726\,916\,40(-2)$	$-0.726\,904\,28(-2)$	$-0.726\,905\,62(-2)$	$-0.726\,905\,82(-2)$
17	$-0.726\,916\,52(-2)$	$-0.726\,916\,47(-2)$		$-0.726\,905\,67(-2)$	
18	$-0.726\,916\,39(-2)$	$-0.726\,916\,45(-2)$		$-0.726\,905\,64(-2)$	
19	$-0.726\,916\,43(-2)$	$-0.726\,916\,45(-2)$			

[a] (-2) denotes the exponents. Thus $-0.726\,916\,98(-2)\equiv -0.726\,916\,98\times 10^{-2}$.

the $l=0$ scale parameter is $\lambda_s=2.0$ [see Eq. (2.5)]. Optimal representation of $l=1,2,\ldots$ functions requires values of λ_l ($l=1,2,\ldots,$) which will overlap strongly with the $1s$ state, suggesting the choice $\lambda_s=\lambda_p=\lambda_d=\cdots=2.0$. Results of a trial calculation with $l=0$, 1, 2, and 3, and with 5 and 10 functions per angular symmetry are shown in Fig. 2, as a function of the complex rotation angle θ. The θ trajectory shown suggests that $\theta=0.4$ rad is a near optimal value for high-precision work and this value is used in the convergence studies shown in Tables I and II. Table I shows convergence as a function of $l_{\max}$, and $N_l=n_s=n_p=n_d=\cdots$, of the imaginary part of the complex eigenvalue corresponding to the broadened and shifted $1s$ state at a field of 0.1 a.u. Examination of the table indicates that convergence to six significant figures has been obtained for $\mathrm{Im}[E_{1s}(F=0.1)]$. Results of similar convergence studies for fields of 0.3, 0.06, and 0.08 a.u. are shown in Table II where they are compared with the Borel-series summation results of Ref. 9 and Padé results of Ref. 8. It is clear that the present convergence studies substantiate the Borel summation of the strongly divergent Rayleigh-Schrödinger expansion to the number of figures given. It is equally clear that the Padé resummation, as carried out in Ref. 8, has only converged to four or five significant figures, rather than the six or seven of the present and Borel methods.

B. Time evolution in a dc field

In the Schrödinger representation, time evolution of an (L^2) state $|\phi\rangle$ at $t=0$ is given by $e^{-iHt}|\phi\rangle$. The amplitude for transition to another L^2 state $|\chi\rangle$ as a function of time is[14,15]

$$\langle\chi|e^{-iHt}|\phi\rangle=\frac{1}{2\pi i}\int_{\mathscr{C}}e^{-izt}\langle\chi,(z-H)^{-1}\phi\rangle \tag{2.8a}$$

this latter being a Laplace-transform representation, with the contour $\mathscr{C}$ enclosing the spectrum of the Hamiltonian H. The reason for introduction of the resolvent $(z-H)^{-1}$ in Eq. (2.9), is that the theory[16] of complex scale transformations, $r\rightarrow re^{i\theta}$, tells us that

$$\langle\chi(\theta),[z-H(\theta)]^{-1}\phi(\theta)\rangle \equiv\langle\chi,U_\theta^{-1}U_\theta(z-H)^{-1}U_\theta^{-1}U_\theta\phi\rangle,$$

U_θ being the unitary operator which introduces the scale transformation, and provides the analytic continuation of $\langle\chi,(z-H)^{-1}\phi\rangle$ into the lower half-plane. Thus,

$$\langle\chi|e^{-iHt}|\phi\rangle=\frac{1}{2\pi i}\int_{\mathscr{C}'}e^{-izt}\langle\chi(\theta),[z-H(\theta)]^{-1}\phi(\theta)\rangle \tag{2.8b}$$

where the new contour $\mathscr{C}'$ can be distorted as shown in Fig. 3. Formally undoing the Laplace transform, we have

$$\langle\chi|e^{-iHt}|\phi\rangle=\langle\chi(\theta)|e^{-iH(\theta)t}|\phi(\theta)\rangle. \tag{2.9}$$

Introduction of a matrix representation of $H(\theta)$ [i.e., $\underline{H}(\theta)$] in an L^2 basis $\{\phi_j\}$, now gives

$$\langle\chi|e^{-iHt}|\phi\rangle\approx\langle\chi(\theta)|e^{-iH(\theta)t}|\phi(\theta)\rangle =\langle\underline{\chi}(\theta)^T|e^{-i\underline{H}(\theta)t}|\underline{\phi}(\theta)\rangle, \tag{2.10}$$

where $\underline{\phi}(\theta)$ and $\underline{\chi}(\theta)$ are the vectors of overlaps $\langle\phi_j|\phi(\bar{\theta})\rangle$ and $\langle\bar{\phi}_j|\chi(\theta)\rangle$, respectively. Assuming that the complex symmetric eigenvalue problem

$$\underline{H}(\theta)\underline{C}_i(\theta)=E_i\underline{C}_i(\theta) \tag{2.11}$$

is solved for the right eigenvectors $\underline{C}_i(\theta)$ and (complex) eigenvalues E_i, we can rewrite (2.10) using the bi-orthogonal spectral resolution

TABLE II. Comparison of complex eigenvalues for the hydrogenic 1s state in dc fields of 0.03, 0.06, 0.08, and 0.10 a.u. as determined by the present complex-coordinate calculations, and by Padé (Ref. 8) and Borel (Ref. 9) summations of the strongly divergent Rayleigh Schrödinger perturbation expansion. Borel method of Ref. 9 has clearly given converged widths to the number of figures given. Parentheses indicate exponents of 10, e.g., $0.7(-2)=0.007$. Pairs of numbers in square brackets, e.g., [12,12] indicates a diagonal Padé approximant of order 12 in numerator and denominator. $\theta=0.4$ in all calculations (see text).

Computational method	$E_{1s}(F)$
$F=0.03$	
Complex coordinate ($l_{max}=11$)	
$n=15$	$-0.502074272\,6-0.111\,881(-7)i$
$n=16$	$-0.502\,074\,272\,6-0.111\,883(-7)i$
Padé sum	
[12,12]	$-0.502\,074\,272\,6-0.111\,90(-7)i$
[13,13]	$-0.502\,074\,272\,6-0.111\,94(-7)i$
Borel sum	$-0.502\,074\,272\,6-0.111\,88(-7)i$
$F=0.06$	
Complex coordinate ($l_{max}=10$)	
$n=17$	$-0.509\,703\,45-0.257\,5389(-3)i$
$n=18$	$-0.509\,203\,45-0.257\,5389(-3)i$
Padé sum	
[12,12]	$-0.509\,203\,60-0.257\,545(-3)i$
[13,13]	$-0.509\,203\,60-0.257\,545(-3)i$
Borel sum	$-0.509\,203\,45-0.257\,538(-3)i$
$F=0.08$	
Complex coordinate ($l_{max}=10$)	
$n=17$	$-0.517\,560\,62-0.226\,9827(-2)i$
$n=18$	$-0.517\,560\,62-0.226\,9827(-2)i$
Padé sum	
[12,12]	$-0.517\,559\,5-0.226\,862(-2)i$
[13,13]	$-0.517\,559\,5-0.226\,865(-2)i$
Borel sum	$-0.517\,560\,62-0.226\,982(-2)i$
$F=0.10$	
Complex coordinate ($l_{max}=11$)	
$n=15$	$-0.527\,418\,173-0.726\,9057(-2)i$
$n=16$	$-0.527\,418\,173-0.726\,9058(-2)i$
Padé sum	
[12,12]	$-0.527\,425-0.727\,062(-2)i$
[13,13]	$-0.527\,425-0.727\,062(-2)i$
Borel sum	$-0.527\,418\,17-0.726\,905(-2)i$

$$\underline{H}(\theta)=\sum_i \underline{C}_i(\theta)E_i\,\underline{C}_i^T \tag{2.12}$$

where $\underline{C}_i^T$, the corresponding left eigenvector, is simply the transpose[4a] (*not* the Hermitian conjugate) of the vector $\underline{C}_i$:

$$\langle\chi\,|\,e^{-iHt}\,|\,\phi\rangle=\sum_i[\underline{\chi}(\theta)]^T\underline{C}_i(\theta)\times e^{-iE_it}[\underline{C}_i(\theta)]^T\underline{\phi}(\theta)\,, \tag{2.13}$$

where $\underline{a}^T\underline{b}$ is the real (i.e., no complex conjugation) scalar product. The discrete sum in Eq. (2.13) contains complex eigenvalues which correspond to identifiable decaying Stark states and the other eigenvalues which give a generalized Gaussian quadrature[17] of the remnants of the continuous spectrum of $H^{\text{Stark}}(\theta)$. To exemplify the utility of Eq. (2.9), and its matrix spectral resolution, Eq. (2.13), we present converged results for the time evolution of the 1s state of atomic hydrogen in the presence of suddenly and adiabatically applied dc Stark fields.

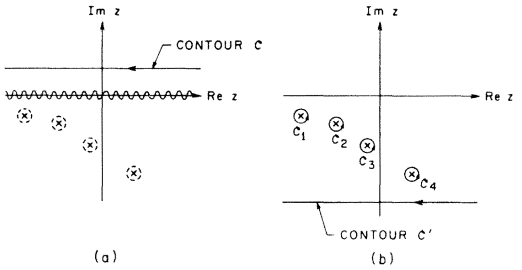

FIG. 3. Contour distortion and evaluation of the Laplace transform of Eqs. (2.8a) and (2.8b). (a) A usual transform inversion contour (see, for example, Ref. 14) is shown. Contour is directed from $+\infty$ to $-\infty$ (positively) in the upper-half plane, and thus encloses the spectrum of the dc Stark Hamiltonian, which is the whole real axis. (b) Applied to the use of $\langle\phi(\theta),[z-H(\theta)]^{-1}\chi(\theta)\rangle$, which gives an identical time evolution; in the transform the continuous spectrum of $H^{\text{Stark}}(\theta)$ has moved into the lower-half plane (see Cerjan *et al.*, Ref. 2 and Herbst, Ref. 13) exposing the Stark resonances. Contour of (a) may then be distorted as shown, resulting in time evolution dominated by the resonance poles, but also including the remaining continuum contributions. These latter are effectively quadratured by the L^2 basis.

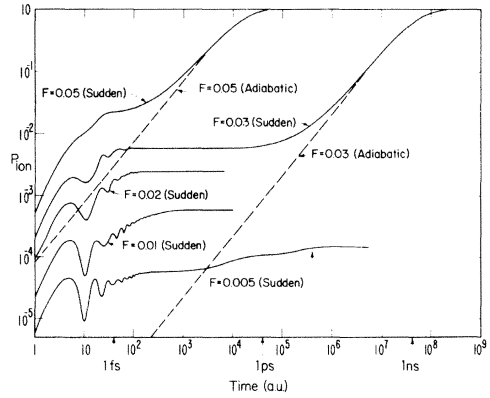

FIG. 4. Time evolution of the hydrogenic 1*s* state in suddenly and adiabatically applied dc Stark fields. Sudden application (i.e., in times less than a few fsec) results in rapid ionization of high-lying Stark states which are populated in the sudden turn-on, resulting in a "plateau" in $P_{\text{ion}}(t)$ hiding the contribution from the more slowly ionizing 1*s* Stark state. In adiabatic turn-on of the field the decay is pure exponential, as only one pole of Fig. 3(b) contributes. At the lowest field ($F=0.005$ a.u.) after initial transients the two $n=2$, $m_l=0$ Stark states resulting from sudden turn-on may be seen to ionize at times $\tau\sim 10^4$ and 2×10^5 a.u.

Figure 4 shows the probability of ionization of ground-state atomic hydrogen for a field turned on at time 0 and turned off at time t. Namely,

$$P_{\text{ion}}(t)\equiv 1-\sum_j |\langle\phi_j|e^{-iH^{\text{Stark}}t}|\phi_0\rangle|^2 , \quad (2.14)$$

where $|\phi_0\rangle$ is the exact ground state of (field-free) hydrogen, and the sum over j includes all bound states of (field-free) atomic hydrogen. The figure indicates the existence of very strong transients for the sudden turn on. These are simply due to population of many high-lying resonances of $H^{\text{Stark}}(\theta)$ at $t=0$ due to the sudden turn-on of the field. These high-lying Stark resonances corresponding to excited states of hydrogen which ionize relatively quickly, giving rise to a constant term in $P_{\text{ion}}(t)$ which visually swamps out the ionization of the population in the slowly ionizing 1*s* state for a substantial period of time. Thus the only physical significance of the "plateau" regions in the sudden turn-on time evolution is that the plateau indicates the total probability of early ionization due to the sudden turn-on. The time scale of the transients in Fig. 4 indicates that the dc field would have to be turned on in the order of less than 0.1 fsec for this structure to be observed. Conversely, adiabatic turn-on gives decay dominated for all times of physical interest by a single exponential. For the case of sudden turn-on Geltman[18] has numerically integrated a one-dimensional model Stark problem obtaining time dependence quite similar to those of Fig. 4.

We thus see that the use of an L^2 expansion basis, and the complex scaled $H^{\text{Stark}}(\theta)$, not only allows computation of individual complex resonance eigenvalues (Sec. II A), but also allows elucidation of quite complicated multiple—time-scale time evolution. Having established the utility of this complex-coordinate matrix technique, we proceed to the case of the ac Stark effect.

III. TIME-INDEPENDENT FLOQUET HAMILTONIAN

The time-dependent Hamiltonian whose dynamics we wish to discuss is, for atomic hydrogen,

$$H(t)=-\frac{\nabla^2}{2}-\frac{1}{r}-Fz\cos(\omega t) \quad (3.1)$$

which describes the interaction of the atom with a monochromatic, linearly polarized, coherent field of frequency ω and peak field strength F. The *time-independent* Hamiltonian, equivalent to that of Eq. (3.1) in the sense that correct *cycle-averaged time evolution* is given by $\exp(-iH_\omega^{\mathcal{F}}t)$ has been given by Shirley[19] (with $\hbar=m_e=e^2=1$)

$$H_\omega^{\mathcal{F}}=-\frac{\nabla^2}{2}-\frac{1}{r}+\omega a_\omega^\dagger a_\omega-\frac{Fz}{2}(a_\omega^\dagger+a_\omega), \quad (3.2)$$

where $a_\omega^\dagger$ (a_ω), are the creation (annihilation) operators for linearly polarized photons (i.e., Floquet-Fourier comments) of frequency ω.[20] As the cycle times in the frequency regions considered in multiphoton ionization are extremely short compared to times of physical interest (e.g., Rabi frequencies and/or ionization "rates") for usual and even high field intensities, the approximation of working with $H_\omega^{\mathcal{F}}$, rather than constructing the complete Floquet time-evolution operator, as recently done by Wyatt *et al.*,[10] is minor compared to the assumption of complete coherence and monochromaticity.

The Floquet Hamiltonian $H_\omega^{\mathcal{F}}$ of Eq. (3.2) and the dc Stark Hamiltonian H^{Stark} of Eq. (2.1) are remarkably similar, suggesting at once that $H_\omega^{\mathcal{F}}$ might be transformed $H_\omega^{\mathcal{F}} \rightarrow H_\omega^{\mathcal{F}}(\theta)$:

$$H_\omega^{\mathcal{F}}(\theta) = -e^{2i\theta}\frac{\nabla^2}{2} - \frac{e^{-i\theta}}{r} + \omega a_\omega^\dagger a_\omega - e^{i\theta}\frac{Fz}{2}(a_\omega^\dagger + a_\omega) \tag{3.3}$$

and that $H_\omega^{\mathcal{F}}(\theta)$, like $H^{\text{Stark}}(\theta)$, of Eq. (2.3) has complex eigenvalues with corresponding complex eigenvectors, whose imaginary parts might be associated with lifetimes of appropriately prepared states, that is with multiphoton-induced time evolution, including ionization. More generally, construction of $e^{-iH_\omega^{\mathcal{F}}(\theta)t}$ is expected to allow discussion of time evolution of arbitrarily prepared states, as in the dc case discussed in Sec. II B. The first of these conjectures was verified by Chu and Reinhardt[2] and subsequently exploited by Chu.[2,21] Exploitation of the ability to treat time evolution is discussed in HRR.[6]

For actual calculations of the L^2 eigenfunctions of $H_\omega(\theta)$, which will correspond to fully dressed states with complex eigenvalues, the atomic states are well represented by the $|\phi_{n,l,m_l}\rangle$ of Eq. (2.4). The presence of the $a_\omega^\dagger a_\omega$ and $(a_\omega^\dagger + a_\omega)$ terms in $H(\theta)$ require extension of the atomic-state space to include photon states, and thus used a direct-product basis, denoted by

$$|n,l,m_l;N\rangle = |\phi_{n,l,m_l}\rangle \otimes |N\rangle , \tag{3.4}$$

where $|N\rangle$ is an N-photon state. In this direct-product basis the Hamiltonians H_ω and $H_\omega(\theta)$ are block tridiagonal in the photon number N, as $(Fz/2)(a_\omega^\dagger + a_\omega)$ only connects states differing by ± 1 photons. Choosing the origin of the energy scale at $E_0 = N\omega$ ($\hbar = 1$), the structure of the matrix representation of $H_\omega^{\mathcal{F}}$ [or $H_\omega^{\mathcal{F}}(\theta)$] is block tridiagonal in photon number $N+M$:

$$\begin{array}{c} \\ \vdots \\ |\{a\};N-2\rangle \\ |\{a\};N-1\rangle \\ |\{a\};N\rangle \\ |\{a\};N+1\rangle \\ |\{a\};N+2\rangle \end{array} \begin{array}{c} \cdots\ |\{a\};N-2\rangle \quad |\{a\};N-1\rangle \quad |\{a\};N\rangle \quad |\{a\};N+1\rangle \quad |\{a\};N+2\rangle \cdots \\ \left[\begin{array}{ccccc} \cdots [N-2] & [V_{-2,-1}] & \underline{0} & \underline{0} & \underline{0} \\ [V_{-1,-2}] & [N-1] & [V_{-1,0}] & \underline{0} & \underline{0} \\ \underline{0} & [V_{0,-1}] & [N] & [V_{0,1}] & \underline{0} \\ \underline{0} & \underline{0} & [V_{1,0}] & [N+1] & [V_{1,2}] \\ \underline{0} & \underline{0} & \underline{0} & [V_{2,1}] & [N+2] \end{array}\right] \end{array} , \tag{3.5}$$

where $\{a\}$ represents a complete set of functions spanning the full manifold of atomic states. The diagonal blocks $[N+M]$, $M = 0, \pm 1, \pm 2, \ldots$, correspond to the unperturbed part of the Hamiltonian $H_0 = H_{\text{atom}} + H_{\text{field}}$. In the basis $\{\alpha_i\}$ of uncoupled (atom) plus field states $|\{\alpha\};N+M\rangle$ the block $[N+M]$ is the diagonal matrix

$$[N+M] = \begin{array}{c} \\ |\alpha_1;N+M\rangle \\ |\alpha_2;N+M\rangle \\ \vdots \\ |\alpha_i;N+M\rangle \\ \vdots \end{array} \begin{array}{c} |\alpha_1;N+M\rangle \quad |\alpha_2;N+M\rangle \quad \cdots \quad |\alpha_i;N+M\rangle \quad \cdots \\ \left[\begin{array}{cccc} E_{\alpha_1}+M\omega & 0 & \cdots & 0 \\ 0 & E_{\alpha_2}+M\omega & & 0 \\ \vdots & \vdots & & \vdots \\ 0 & 0 & \cdots & E_{\alpha_i}+M\omega \\ \vdots & \vdots & & \vdots \end{array}\right] \end{array} , \tag{3.6}$$

where E_{α_i} is the energy of the atomic state $|\alpha_i\rangle$ and ω is the frequency of the laser field. In the complete discrete basis $|i;N\rangle \equiv |n_i,l_i,m_{l_i};N\rangle$ of Eq. (3.4) $[N+M]$ has the structure

$$\langle i;O\,|\,[N+M]\,|\,j;O'\rangle = [\langle i\,|\,H^{\text{atom}}\,|\,j\rangle + (N+M)\omega]\delta_{O,N+M}\delta_{M+N,O'} . \tag{3.7}$$

The off-diagonal blocks of Eq. (3.5) are of the form

$$[V_{M,M\pm1}]_{ij}=\langle a_i;N+M \mid V^{\text{atom}-\text{photon}} \mid a_j;N+M\pm1\rangle \tag{3.8a}$$

and in the limit of large photon-occupation numbers are proportional to $\sqrt{N+M}\approx\sqrt{N+M\pm1}\approx\sqrt{N}$ which is the dimensionless classical amplitude of the field, allowing Eq. (3.8a) to be rewritten

$$[V_{M,M\pm1}]_{ij}=\frac{F}{2}\langle a_i \mid z \mid a_j\rangle \ . \tag{3.8b}$$

In this limit the semiclassical Floquet theory and quantized field Hamiltonians are identical.[19]

In what follows, converged eigenvalues of the matrix (3.5) corresponding to $H_\omega^{\mathcal{F}}(\theta)$ will be found. However, before discussing calculations we note that most atom plus field states are uncoupled in the dipole approximation which we henceforth assume. If we assume an initial state, atomic field $|n_0,l_0,m_{l_0};N\rangle$ of definite angular momentum l_0, and parity $(-1)^{l_0}$ whose time evolution is of interest, the dipole selection rules appropriate to linear polarization require that coupling can only occur between states which differ by ±1 units of angular momentum. Thus, for example, the atomic hydrogenic states $\langle 1s;N\mid,\langle 1s;N+1\mid,\langle 1s;N-1\mid,$ $\langle 1s;N+3\mid,\langle 1s;N-3\mid,\ldots,$ are uncoupled. Assuming an initial hydrogenic state of s symmetry the block structure of Eq. (3.5) collapses to that shown in Fig. 5 where only those atom plus field states of symmetry appropriate to coupling to states of the form $|n,l=0,m_l=0;N\rangle$ are shown. The block-matrix structure of Eq. (3.9) is the direct generalization of the structure of Eqs. (2.6) and Fig. 1 to the ac Stark case. The off-diagonal blocks $[V_{l,l\pm1}]$ are those of Eq. (2.6c) and the diagonal blocks are those of Eq. (2.6a) augmented by $M\omega\delta_{ij},M=0,\pm1,\pm2,\ldots$. The block matrix of Fig. 5 is enormously simpler in structure than that of Eq. (3.5), even though no approximations have been made. The collapse indicated in Fig. 5 is equivalent to full utilization of symmetry relations in the more usual statements of Floquet theory.[22]

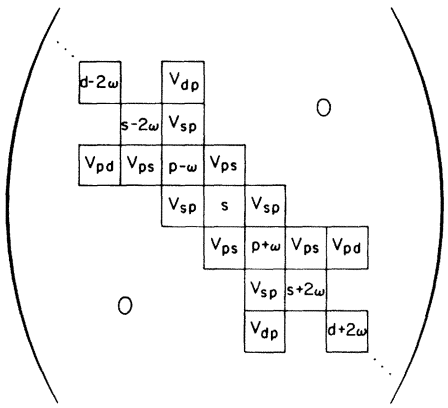

FIG. 5. ac Stark block-matrix structure arising directly from the structure of $H_\omega^{\mathcal{F}}$ [or $H_\omega^{\mathcal{F}}(\theta)$] of Eq. (3.3) or (3.5) if the initial state to be propagated is of the type $|n,l=0,m_l=0;N\rangle$. That is an atomic s state. As all N-photon direct product states with $l\neq0$ have zero overlap with $|n,l=0,m_l=0,N\rangle$ all of these states and all of those connected to them by 1,2,..., M-photon processes play no role in the time evolution, and thus may simply be omitted, resulting in the collapsed form shown here.

A slightly rearranged version of the block-matrix structure of Fig. 5 will be used in discussions of computational applications, while the full block-matrix structure of Eq. (3.5) will be used in making formal contact with previously derived continued-fraction representations[1] of multiphoton transition amplitudes.

IV. ac STARK PROBLEM: CALCULATION OF COMPLEX DRESSED EIGENVALUES

In this section it is shown that complex eigenvalues corresponding to complex dressed states are easily converged using modest expansions in L^2 functions and in "M" which measures the excursions in photon number from an initial photon state N. Section IV A details numerical convergence, and IV B briefly discusses the blockwise inverse iteration used to locate complex eigenvalues with a minimum of storage and computational effort. As will become clear in this latter discussion it is advantageous for computations to rearrange the ordering of blocks in the collapsed Floquet Hamiltonian as is indicated in Fig. 6. The analogous block-matrix structure for circular polarization has been given by Chu.[2] Again, no approximations are involved; the block-matrix structure of Figs. 5 and 6 are related by simply reindexing. It is the block-matrix structure of Fig. 6 which will be used in all succeeding discussions of computational results. Each of the blocks of type A reduces to the dc Stark case as $\omega\rightarrow0$, and we refer to *each* as a *Floquet block.*

A. Choices of parameters and demonstration of convergence

As indicated in Sec. III we expect to find complex eigenvalues of the matrix representation of $H_\omega^{\mathcal{F}}(\theta)$. The matrix representation is completely specified by the choice of basis functions, the number of atomic symmetries, and by the number of Floquet blocks to be included. Appropriate choices of all of these will be a function of field strength, and of the frequency

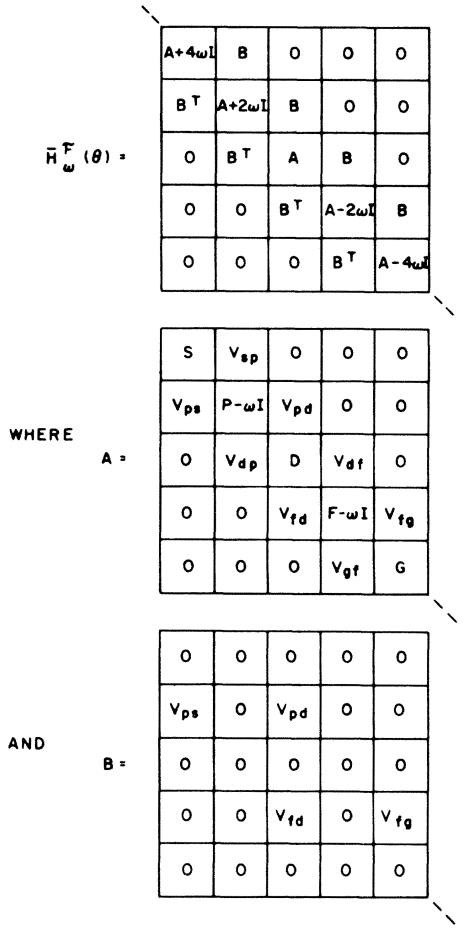

FIG. 6. Rearranged block-matrix structure of the Floquet matrix of Fig. 5, in a form most suitable for numerical applications. This follows from the fact that only the matrices $\underline{A}$ and $\underline{B}$ need be stored, and that the tridiagonal structure may be exploited (see the Appendix). This form of the matrix is that used earlier by Chu and Reinhardt (Ref. 2), generalization to circular polarization has been given by Chu (Ref. 2).

ω. We consider two quite simple examples—more complicated examples are considered in HRR.[6]

For atomic hydrogen at external fields of low intensity and for frequencies $\omega \geq 0.5$ a.u., only ordinary single-photon ionization ($1s \rightarrow kp$) can occur with any real probability. If only one photon $s \rightarrow p$ absorption is of importance only one Floquet block need be considered, and only s and p blocks included in that single block. One expects to find a complex eigenvalue near $-\frac{1}{2}$ with a shift and width corresponding to the real and imaginary parts of the frequency-dependent polarizability $\alpha(\omega)$. However, given that only two l symmetries need be included how are the nonlinear scale parameters λ and θ chosen? The dressed eigenvectors will be approximately a $1s$ hydrogenic function, suggesting a value of $\lambda = \lambda_s = \lambda_p$ of 1 or 2. The optimal value of θ may then be determined empirically. Figure 7 shows relative convergence of the imaginary part of the complex dressed $1s$ state of hydrogen for $\omega = 0.6$ a.u. and $F = 10^{-4}$ a.u. It is evident that a value of $\theta \simeq 0.45$ rad is optimal in this case although if results are required only to three or four significant figures any value of θ between 0.3 and 0.6 is satisfactory. The converged complex eigenvalue at $F = 10^{-4}$, $\omega = 0.6$ is $E_{1s} = -0.499\,998\,940\,826 - 0.626\,2659 \times 10^{-6} i$, which converges to the number of figures given. Conversion of the imaginary part of this energy level into a cross section gives the usual one-photon photoeffect cross section to the number of figures quoted; see also the discussions of Ref. 5 for complex-coordinate calculations of one-photon ionization cross sections.

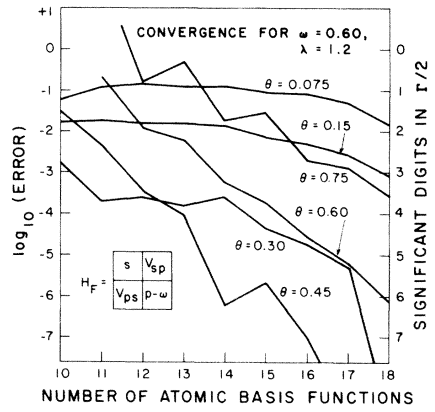

FIG. 7. Convergence studies of the shifted and broadened hydrogenic $1s$ state in an ac field of frequency 0.6 a.u., and at an intensity low enough to ensure that only the usual one-photon photoeffect is of importance. Plotted is $\log_{10}(|\Gamma/2 - \Gamma/2^{\text{exact}}|)$ where $\Gamma/2$ is the width resulting from the finite-dimensional–matrix calculation described in the text. For these illustrative calculations $\lambda = 1.2$ and $N = n_s = n_p$ the number of basis functions of each symmetry is varied for a range of values of θ. It is evident that for θ in the range from 0.3 to 0.6 rad that rapid convergence is easily obtained. While it is rarely of importance to calculate a cross section to more than two or three significant figures, the present results indicate that systematically convergent results of very high accuracy can be obtained from such a finite L^2 basis computation. In this particular case, the photoeffect cross section can be analytically extracted from the same L^2 basis without use of complex coordinates as discussed in Yamani and Reinhardt, Ref. 3. In the multiphoton case use of complex coordinates enormously simplifies treatment of overlapping strongly coupled continua.

As a second example of convergence consider $F_{\rm rms}=F/\sqrt{2}=0.025$ a.u., and $\omega=0.375$ a.u. At this frequency the uncoupled states $1s$ and $2p-\omega$ (i.e., the states $|1,0,0;N\rangle$ and $|2,1,0;N-1\rangle$ in the exact atomic basis) are degenerate and we expect the processes $1s\rightarrow(2p-\omega)\rightarrow(ks-2\omega)$ and $(kd-2\omega)$ to be important. Thus, strongly resonant two-photon ionization will dominate at low fields, and additional processes may well enter at higher fields. Thus at least two and perhaps more Floquet blocks are needed, and a minimum description involves use of atomic orbitals of s,p,d symmetry. Figures 8 and 9 show relative convergence for the imaginary part of the dressed $1s$ state under these conditions as a function of $\lambda=\lambda_s=\lambda_p=\lambda_d$, θ, and the number of atomic basis functions ($N=n_s=n_p=n_d$) for a series of calculations involving three Floquet blocks and the s,p,d atomic symmetries. Specific values of the widths appear in Table III. Table IV indicates that at this relatively high field ($F_{\rm rms}=0.025$ corresponds to an rms intensity of $\sim 6\times 10^{12}$ W/cm^2), inclusion of the Floquet blocks with A, $A\pm 2\omega$, and $A-4\omega$ was necessary to achieve convergence indicating minor importance (3% to 4%) of four-photon as well as two-photon processes at this intensity. The relationship of these converged widths to actual rates of multiphoton process is discussed in Sec. VI of this paper, and in HRR.

B. Numerical determination of complex eigenstates

The block-matrix structure indicated in Fig. 6 suggests that it should be possible to carry out calculations with only the necessity of calculation of the single Floquet block A, and the sparse coupling block B. *This is, in fact, the case and implies that the size of actual matrix computation depends only on the number of atomic basis states needed to describe the problem at hand.* This latter is almost always a much smaller number than the dimensionality, of the block-matrix truncated Floquet Hamiltonians. Thus, for the five-block s,p,d,f,g calculation discussed in the caption to Table III the maximum matrix to be stored was a 75×75 complex-value symmetric matrix which is itself block tridiagonal, further reducing storage requirements.

Actual complex eigenvalues were determined by a blockwise inverse iteration procedure taking full advantage of the block-matrix structure in both storage and the computational algorithm. The general strategy of the algorithm used is outlined in the Appendix. The fact that storage and computational requirements scale as the cube of the numbers of atomic states, and linearly in the number of Floquet blocks, rather than the cube of the dimensionality of the truncated Floquet matrix indicates that the method has the same basic computational advantages as the numerical Floquet method recently introduced by Wyatt *et al.*[10] The main difference be-

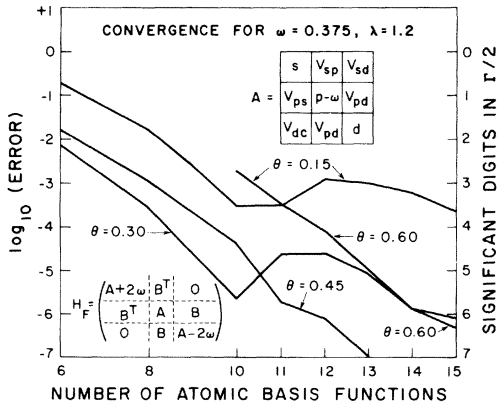

FIG. 8. Convergence of the width of the hydrogenic $1s$ state in a case where resonant two-photon ionization is possible. States of three atomic symmetries, and three Floquet blocks are included. For $\lambda=1.2$, convergence as a function of $n=n_s=n_p=n_d$ is shown for a range of values of θ.

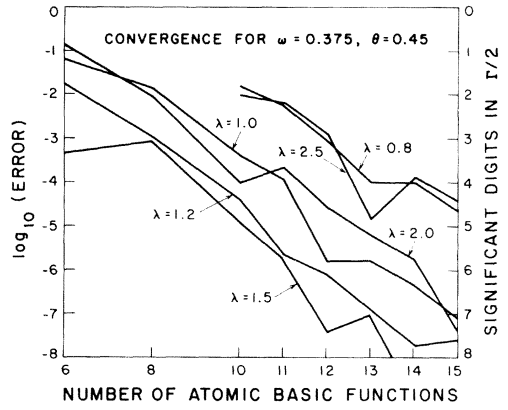

FIG. 9. Convergence of $\mathrm{Im}(E_{1s})$ for the case discussed in Fig. 8. In this case θ is held fixed at 0.45 rad, and convergence investigated for several values of λ. Inspection of this figure and Fig. 8 leads to the conclusion that λ in the range $1.2-2.0$, and θ in the range $0.30-0.60$ is adequate for most purposes. This clearly indicates that the choice of these parameters is not particularly critical as long as ≈ 10 basis functions per atomic symmetry are used. Successful performance of calculations with significantly smaller numbers of atomic functions is possible but requires careful simultaneous nonlinear optimization of θ and λ or, equivalently, inclusion of complex values of θ [see, for example, E. Brändas and P. Froelich, Phys. Rev. A 16, 2207 (1977)].

TABLE III. Convergence of the imaginary part $\Gamma/2$ of the broadened and shifted "1s" state of H in the presence of a linearly polarized laser field with $\omega=0.375$ implying an exact zeroth-order resonance 1s, $2p-\omega$, and thus a width dominated by two-photon ionization. Convergence is shown for representative values of the nonlinear parameters θ and λ, as a function of N, the number of atomic functions of each symmetry. For these calculations $N_{\mathcal{F}}=3$ and $F_{\rm rms}=0.025$ a.u., a strong external field. Examination of these results and those of Figs. 8 and 9 indicates both that results of 1% precision are quite easily obtained for a wide range of parameters and basis sizes, and that results of very high precision can be obtained if needed. Effect of inclusion of additional Floquet blocks, needed at this high field, is documented in Table IV.

	Nonlinear parameters		
N[a]	$\theta=0.30,\lambda=1.2$	$\theta=0.54,\lambda=1.2$	$\theta=0.45,\lambda=1.5$
6	0.141 790 85(−3)	0.120 160 69(−3)	0.135 157 46(−3)
8	0.134 918 25(−3)	0.135 693 92(−3)	0.133 590 70(−3)
10	0.134 642 03(−3)	0.134 595 88(−3)	0.134 627 88(−3)
11	0.134 616 51(−3)	0.134 641 47(−3)	0.134 635 71(−3)
12	0.134 616 51(−3)	0.134 638 69(−3)	0.134 639 52(−3)
13	0.134 648 70(−3)	0.134 639 38(−3)	0.134 639 38(−3)
14	0.134 638 09(−3)	0.134 639 50(−3)	0.134 639 48(−3)
15	0.134 638 60(−3)	0.134 639 45(−3)	0.134 639 48(−3)

[a]n is the number of atomic basis functions of each symmetry. In the present calculation $n_s=n_p=n_d=N$, and the dimension of a single Floquet block of type "A" is thus $(3N\times 3N)$. As the blocks A, $A-2\omega$, and $A+2\omega$ are included, the total matrix has dimension $(9N\times 9N)$ which ranges from 54×54 to 135×135 for these convergence studies. However, see the Appendix for a discussion of the effective size of the computations.

tween the approaches is that Wyatt and co-workers construct the full Floquet propagator, while we construct the cycle-averaged propagator. We also note use of a subset of a complete discrete basis, rather than actual atomic eigenstates, can be related to the Dalgarno-Lewis method, and that the block-matrix manipulations discussed in the Appendix can be directly related (the difference being presence or absence of complex coordinates in addition to use of finite-dimensional—matrix techniques involving ex-

TABLE IV. Overall view of convergence of E_{1s} for the resonant frequency $\omega=0.375$ a.u. and $F(\text{rms})=0.025$ a.u. showing the convergence (to five figures in $i\Gamma/2$) as a function of rotation angle θ, basis scale parameter λ, number of Floquet blocks N, number of atomic basis functions, and number of atomic angular symmetries. Where the scale parameter is indicated as 1.2(1.5), the indicated change in exponent does not affect the figures shown. For the $15s,15p,15d,15f,15g$ calculation with five Floquet blocks, the eigenvalue was obtained from a complex symmetric matrix of dimension 375×375. In contrast, as documented in Figs. 8 and 9 results good to 3% in $i\Gamma/2$ can be obtained from an $N=3$ calculation of dimension as small as 54×54 using optimized values of θ and λ. Thus large-scale calculations are usually only needed to check convergence, or to obtain high-precision results.

Basis	λ	θ (rad)	N	E_{1s}	
15s 15p 15d	1.2	0.45	3	−0.511 946	$-1.3464\times 10^{-4}i$
	1.5	0.5236	3	−0.511 946	$-1.3464\times 10^{-4}i$
15s 15p 15d 15f	1.2(1.5)	0.45	4	−0.511 923	$-1.3827\times 10^{-4}i$
	1.2(1.5)	0.5236	4	−0.511 923	$-1.3827\times 10^{-4}i$
10s 10p 10d 10f 10g	1.2(1.5)	0.45	5	−0.511 923	$-1.3824\times 10^{-4}i$
13s 13p 13d 13f 13g	1.2(1.5)	0.45	5	−0.511 923	$-1.3827\times 10^{-4}i$
15s 15p 15d 15f 15g	1.2(1.5)	0.45	5	−0.511 923	$-1.3827\times 10^{-4}i$
	1.2(1.5)	0.5236	5	−0.511 923	$-1.3827\times 10^{-4}i$

pansion in an L^2 set) to the recent discussions of Gontier, Rahman, and Trahin[23] who have explicitly introduced the Dalgarno-Lewis[25] technique, and successive solutions of linear equations to construct sums over intermediate states in continued-fraction perturbation theory. We may also note that the method of Ref. 23, if implemented in a finite basis without coordinate rotation, closely related to that of Karplus and Kolker[24] derived in the context of calculation of the frequency-dependent polarizability.

V. RELATIONSHIP TO CONTINUED-FRACTION PERTURBATION THEORY

The strong connections existing between the resolvent operator methods, continued-fraction perturbation theory and the matrix Floquet Hamiltonian approach may be conveniently displayed by making explicit the analytical structure of the elements of the inverse matrix $(z\underline{\mathbb{1}}-\underline{H}_\omega^{\mathcal{F}})^{-1}$. A convenient technique, which takes full advantage of the block-matrix structure of $\underline{H}$ is a standard matrix partitioning technique,[26-28] corresponding to the introduction of the concept of an effective Hamiltonian.[26,29]

In a first step, we examine an elastic transition, i.e., one of the form $\langle a;N\,|\,G(E)\,|\,a;N\rangle$, where the atomic state a might be either an actual atomic eigenstate of an L^2 basis function of the type of Eq. (2.4), and $\underline{G}(E)=(E\underline{\mathbb{1}}-\underline{H}_\omega)^{-1}$. The amplitude itself is of interest for describing forward-scattering processes and may be used in light-shift calculations. Poles of the analytically continued amplitude correspond to the complex eigenvalue of $\underline{H}_\omega(\theta)$, allowing analysis of time evolution.

A. Elastic transition amplitude

To calculate an amplitude of the form $\langle a;N\,|\,(E\underline{\mathbb{1}}-\underline{H}_\omega^{\mathcal{F}})^{-1}\,|\,a;N\rangle$, which is related by Laplace transform to $\langle a;N\,|\,e^{-iH_\omega^{\mathcal{F}}t}\,|\,a;N\rangle$, and thus to time evolution of an initial state, it is convenient to partition the Hamiltonian matrix $(E\underline{\mathbb{1}}-\underline{H})$, as follows:

$$(E\underline{\mathbb{1}}-\underline{H})=\begin{bmatrix}(E\underline{\mathbb{1}}-\underline{H})_{-1,-1} & (E\underline{\mathbb{1}}-\underline{H})_{-1,0} & \underline{0}\\ (E\underline{\mathbb{1}}-H)_{0,-1} & [N] & (E\underline{\mathbb{1}}-\underline{H})_{0,1}\\ \underline{0} & (E\underline{\mathbb{1}}-\underline{H})_{1,0} & (E\underline{\mathbb{1}}-\underline{H})_{1,1}\end{bmatrix}, \tag{5.1}$$

where $\underline{H}\equiv\underline{H}_\omega^{\mathcal{F}}$ or $\underline{H}_\omega^{\mathcal{F}}(\theta)$. Here $[N]$ is the block of $(E\underline{\mathbb{1}}-\underline{H})$ defined by taking all states of N photons. More precisely, in the simple case of a H atom initially in an S state (or in any state with even-parity angular momentum) the block matrix $[N]$ is projected onto the space spanned by the states $|\{s,d,\ldots\};N\rangle$. The diagonal block $(E\underline{\mathbb{1}}-\underline{H})_{1,1}$ is the following infinite partitioned matrix:

$$(E\underline{\mathbb{1}}-\underline{H})_{1,1}=\begin{array}{c}\\ |\{p,f,\ldots\};N+1\rangle\\ |\{s,d,\ldots\};N+2\rangle\\ |\{p,f,\ldots\};N+3\rangle\\ \cdots\end{array}\begin{array}{c}\begin{array}{cccc}|\{p,f,\ldots\};N+1\rangle & |\{s,d,\ldots\};N+2\rangle & |\{p,f,\ldots\};N+3\rangle & \cdots\end{array}\\ \begin{bmatrix}[N+1] & [V_{2,1}] & \underline{0} & \cdots\\ [V_{2,1}] & [N+2] & [V_{2,3}] & \cdots\\ \underline{0} & [V_{3,2}] & [N+3] & \cdots\end{bmatrix}\end{array}, \tag{5.2}$$

where the structure of matrix blocks $[N+M]$ and $[V_{M,M\pm1}]$ is that of Eqs. (3.6)–(3.8).

The nondiagonal infinite matrix blocks denoted $(E\underline{\mathbb{1}}-\underline{H})_{0,1}$ and $(E\underline{\mathbb{1}}-\underline{H})_{1,0}$ assume, respectively, the corresponding forms

$$(E\underline{\mathbb{1}}-\underline{H})_{0,1}=\begin{array}{c}\\ |\{s,d,\ldots\};N\rangle\end{array}\begin{array}{c}\begin{array}{cccc}|\{p,f,\ldots\};N+1\rangle & |\{s,d,\ldots\};N+2\rangle & |\{p,f,\ldots\};N+3\rangle & \cdots\end{array}\\ \begin{pmatrix}[V_{0,1}] & \underline{0} & \underline{0} & \cdots\end{pmatrix}\end{array} \tag{5.3a}$$

and

$$(E\underline{\mathbb{1}}-\underline{H})_{1,0}=\begin{array}{c}\\ |\{p,f,\ldots\};N+1\rangle\\ |\{s,d,\ldots,\};N+2\rangle\\ |\{p,f,\ldots\};N+3\rangle\\ \cdots\end{array}\begin{array}{c}|\{s,d,\ldots\};N\rangle\\ \begin{bmatrix}[V_{1,0}]\\ \underline{0}\\ \underline{0}\\ \cdots\end{bmatrix}\end{array}. \tag{5.3b}$$

The structure of the other matrix blocks can be obtained from the preceding ones by simple symmetry considerations.

The amplitude of interest here, corresponding to an elastic transition, is of the general form $\langle a;N\,|\,(E\underline{1}-\underline{H})^{-1}\,|\,a;N\rangle$, where in our case, the atomic state involved is $|\,a\rangle=|\,\{s,d,\ldots\}\rangle$. As a consequence the full structure of the inverse matrix $(E\underline{1}-\underline{H})^{-1}$ is not needed: only its projection onto the space spanned by the set of vectors $|\,\{s,d,\ldots\};N\rangle$ is required. This determination may be conveniently achieved by using standard block-matrix manipulations.[26,27]

For instance, we solve first the following system:

$$(E\underline{1}-\underline{H})\underline{X}=\underline{Y}\ , \tag{5.4}$$

which, after partitioning according to Eq. (5.1), may be written as

$$(E\underline{1}-\underline{H})_{-1,-1}\underline{X}_{-1}+(E\underline{1}-\underline{H})_{-1,0}\underline{X}_0=\underline{Y}_{-1}\ , \tag{5.5a}$$

$$(E\underline{1}-\underline{H})_{0,-1}\underline{X}_{-1}+[N]\underline{X}_0+(E\underline{1}-\underline{H})_{0,1}\underline{X}_1=\underline{Y}_0\ , \tag{5.5b}$$

$$(E\underline{1}-\underline{H})_{1,0}\underline{X}_0+(E\underline{1}-\underline{H})_{1,1}\underline{X}_1=\underline{Y}_1\ . \tag{5.5c}$$

As we only need to know the structure of the block

$$\langle\{s,d,\ldots\};N\,|\,(E\underline{1}-\underline{H})^{-1}\,|\,\{s,d,\ldots\};N\rangle=[(E\underline{1}-\underline{H})^{-1}]_{0,0}$$

projected onto the space spanned by vectors $|\,\{s,d,\ldots\};N\rangle$ in the inverse matrix $(E\underline{1}-\underline{H})^{-1}$, one may solve the system, Eq. (5.5), with respect to $\underline{X}_0$. The diagonal block-matrices are nonsingular, and one has successively

$$\underline{X}_{-1}=[(E\underline{1}-\underline{H})_{-1,-1}]^{-1}[\underline{Y}_{-1}-(E\underline{1}-\underline{H})_{-1,0}\underline{X}_0]\ , \tag{5.6}$$

$$\underline{X}_1=[(E\underline{1}-\underline{H})_{1,1}]^{-1}[\underline{Y}_1-(E\underline{1}-\underline{H})_{1,0}\underline{X}_0]\ , \tag{5.7}$$

and, replacing in Eq. (5.5b);

$$\begin{aligned}\{[N]-(E\underline{1}-\underline{H})_{0,-1}[(E\underline{1}-\underline{H})_{-1,-1}]^{-1}(E\underline{1}-\underline{H})_{-1,0}-(E\underline{1}-\underline{H})_{0,1}[(E\underline{1}-\underline{H})_{1,1}]^{-1}(E\underline{1}-\underline{H})_{1,0}\}\,\underline{X}_0\\ =-(E\underline{1}-\underline{H})_{0,-1}[(E\underline{1}-\underline{H})_{-1,-1}]^{-1}\underline{Y}_{-1}+\underline{Y}_0-(E\underline{1}-\underline{H})_{0,1}[(E\underline{1}-\underline{H})_{1,1}]^{-1}\underline{Y}_1\ .\end{aligned} \tag{5.8}$$

The needed block element $[(E\underline{1}-\underline{H})^{-1}]_{0,0}$ is merely the coefficient of $\underline{Y}_0$ in the preceding expression for $\underline{X}_0$, namely,

$$\begin{aligned}\langle\{s,d,\ldots\};N\,|\,(E\underline{1}-\underline{H})^{-1}\,|\,\{s,d,\ldots\};N\rangle&=[(E\underline{1}-\underline{H})^{-1}]_{0,0}\\ &=\{[N]-(E\underline{1}-\underline{H})_{0,-1}[(E\underline{1}-\underline{H})_{-1,-1}]^{-1}(E\underline{1}-\underline{H})_{-1,0}\\ &\quad-(E\underline{1}-\underline{H})_{0,1}[(E\underline{1}-\underline{H})_{1,1}]^{-1}(E\underline{1}-\underline{H})_{1,0}\}^{-1}\ .\end{aligned} \tag{5.9}$$

The essential result obtained by this simple partitioning analysis is that the diagonal block-matrix $[(E\underline{1}-\underline{H})^{-1}]_{0,0}$ of the inverse matrix $(E\underline{1}-\underline{H})^{-1}$ is expressed in terms of inverses of the (nonsingular) matrices denoted $(E\underline{1}-\underline{H})_{-1,-1}$ and $(E\underline{1}-\underline{H})_{1,1}$, [Eq. (5.2)]. This result may be easily related to those of Ref. 1. For instance, the block matrix $[(E\underline{1}-\underline{H})^{-1}]_{0,0}$ corresponds to the Green's-function operator denoted G_N in Yeh and Stehle's 1977 paper[1]; the inverse matrices $[(E\underline{1}-\underline{H})_{-1,-1}]^{-1}$ and $[(E\underline{1}-\underline{H})_{1,1}]^{-1}$ are Yeh and Stehle's projected operators denoted, respectively, G_{N-1} and G_{N+1}; the matrices $(E\underline{1}-\underline{H})_{0,1}$ and $[E\underline{1}-\underline{H}]_{1,0}$ correspond to the operators P_NVP_{N+1} and $P_{N+1}VP_N$.

It is an easy matter to check, by simply using block-matrix multiplication rules, that the product $(E\underline{1}-\underline{H})_{0,1}[(E\underline{1}-\underline{H})_{1,1}]^{-1}(E\underline{1}-\underline{H})_{1,0}$ is, as expected, a block matrix defined only on the subspace spanned by vectors belonging to the subset $|\,\{s,d,\ldots\};N\rangle$. Moreover it can be verified that one does not need to know the whole structure of the inverse matrix $[(E\underline{1}-\underline{H})_{1,1}]^{-1}$, only its leading block projected into the space spanned by the vectors $|\,\{p,f,\ldots\};N+1\rangle$.

The required leading block matrix of $[(E\underline{1}-\underline{H})_{1,1}]^{-1}$ may be obtained by further use of the partitioning techniques. Thus,

$$(E\underline{1}-\underline{H})_{1,1}=\begin{bmatrix}[N+1] & (E\underline{1}-\underline{H})_{1,2}\\ (E\underline{1}-\underline{H})_{2,1} & (E\underline{1}-\underline{H})_{2,2}\end{bmatrix}\ , \tag{5.10}$$

where

$$(E\underline{\mathbb{1}}-\underline{H})_{2,2}=\begin{array}{c} \\ |\{s,d,\ldots\};N+2\rangle \\ |\{p,f,\ldots\};N+3\rangle \\ |\{s,d,\ldots\};N+4\rangle \\ \cdots \end{array}\begin{array}{c} \begin{array}{ccc} |\{s,d,\ldots\};N+2\rangle & |\{p,f,\ldots\};N+3\rangle & |\{s,d,\ldots\};N+4\rangle \end{array} \\ \begin{pmatrix} [N+2] & [V_{2,3}] & \underline{0} & \cdots \\ [V_{3,2}] & [N+3] & [V_{3,4}] & \cdots \\ \underline{0} & [V_{4,3}] & [N+4] & \cdots \end{pmatrix} \end{array} \tag{5.11}$$

and

$$(E\underline{\mathbb{1}}-\underline{H})_{1,2}=\begin{array}{c} \\ |\{p,f,\ldots\};N+1\rangle \end{array}\begin{array}{c} \begin{array}{ccc} |\{s,d,\ldots\};N+2\rangle & |\{p,f,\ldots\};N+3\rangle & |\{s,d,\ldots\};N+4\rangle \end{array} \\ \begin{pmatrix} [V_{1,2}] & \underline{0} & \underline{0} & \cdots \end{pmatrix} \end{array} \tag{5.12}$$

with a similar rectangular block matrix representing $(E\underline{\mathbb{1}}-\underline{H})_{2,1}$.

Denoting the leading block matrix of $[(E\underline{\mathbb{1}}-\underline{H})_{1,1}]^{-1}$ projected onto the subspace $|\{p,f,\ldots\};N+1\rangle$ by

$$\{[(E\underline{\mathbb{1}}-\underline{H})_{1,1}]^{-1}\}_{1,1}=\langle\{|p,f,\ldots\};N+1|[(E\underline{\mathbb{1}}-\underline{H})_{1,1}]^{-1}|\{p,f,\ldots\};N+1\rangle\,, \tag{5.13}$$

we have

$$\{[(E\underline{\mathbb{1}}-\underline{H})_{1,1}]^{-1}\}_{1,1}=\{[N+1]-(E\underline{\mathbb{1}}-\underline{H})_{1,2}[(E\underline{\mathbb{1}}-\underline{H})_{2,2}]^{-1}(E\underline{\mathbb{1}}-\underline{H})_{2,1}\}^{-1}\,. \tag{5.14}$$

Again, as we need only the projection of $[(E\underline{\mathbb{1}}-\underline{H})_{2,2}]^{-1}$ onto the space spanned by the vectors $|\{s,d,\ldots\};N+2\rangle,\ldots,$ we may continue to iterate the procedure to recover the continued-fraction structure of the expansion of the block matrix $\{[(E\underline{\mathbb{1}}-\underline{H})_{1,1}]^{-1}\}_{1,1}$ in the expression $[(E\underline{\mathbb{1}}-\underline{H})^{-1}]_{0,0}$ in Eq. (5.9). We have, finally,

$$\langle\{p,f,\ldots\};N+1|[(E-H)_{1,1}]^{-1}|\{p,f,\ldots\};N+1\rangle$$
$$=\left\langle\{p,f,\ldots\};N+1\left|\cfrac{1}{[N+1]-(E\underline{\mathbb{1}}-\underline{H})_{1,2}\cfrac{1}{[N+2]-(E\underline{\mathbb{1}}-\underline{H})_{2,3}\cfrac{1}{[N+3]-\cdots}(E\underline{\mathbb{1}}-\underline{H})_{3,2}}(E\underline{\mathbb{1}}-\underline{H})_{2,1}}\right|\{p,f,\ldots\};N+1\right\rangle. \tag{5.15}$$

The same analysis may be performed also for the symmetrical block matrix $(E\underline{\mathbb{1}}-\underline{H})_{-1,-1}$, which completes the calculation and permits one to recover the main results of Ref. 1.

It should be pointed out that the possibility of obtaining such a compact result is a direct consequence of the symmetry properties of the Hamiltonian matrix [Eq. (3.5)]. Of course, these symmetries are already contained in the model (single mode laser, dipole approximation, etc.) chosen for describing the physical system under consideration, but the matrix method used here permits us to fully exploit these model characteristics.

The expression Eq. (5.15) generalizes the notion of the J fraction[30] to the case where the elements are (noncommutative) matrices. This follows from the fact that the partitioned matrix $(E\underline{\mathbb{1}}-\underline{H})_{1,1}$ [Eq. (5.2)] exhibits the structure of a J matrix whose elements would be matrices themselves. Now it is known, from the theory of the ordinary J matrix with scalar elements, that the leading element $(\underline{J}^{-1})_{1,1}$ of its reciprocal may be expanded as a continued J fraction[30]:

$$\underline{J}=\begin{bmatrix} \alpha_{11} & \alpha_{12} & 0 \\ \alpha_{21} & \alpha_{22} & \alpha_{23} \\ 0 & \alpha_{32} & \alpha_{23} \end{bmatrix};$$
$$(\underline{J}^{-1})_{1,1}=\cfrac{1}{\alpha_{11}-\cfrac{\alpha_{12}\alpha_{21}}{\alpha_{22}-\cfrac{\alpha_{23}\alpha_{32}}{\alpha_{33}-\cdots}}}\,. \tag{5.16}$$

It follows that Eq. (5.15) may be obtained directly from this analysis without resorting to a new partitioning of $(E\underline{\mathbb{1}}-\underline{H})_{1,1}$ as performed in Eq. (5.10). It is sufficient to extend the relations Eq. (5.16) to the case where elements α_{ij} are matrices, provided care is taken to properly define right- or left-handed operations. Similar procedures have previously been used in some extensions of the Padé-approximant

theory.[31-33] More detailed accounts and specialized applications of matrix continued fractions and Padé approximants may be found in these references.

B. Inelastic transition amplitude

Nondiagonal blocks of the inverse matrix $(E\underline{1}-\underline{H})^{-1}$ may be obtained from a slight extension of the matrix partitioning technique described above. It should be noticed first that amplitudes relevant for one-photon transitions can be derived directly from the results of Sec. IV A. For instance, the blocks

$$\langle\{s,d,\ldots\};N\,|\,(E\underline{1}-\underline{H})^{-1}\,|\,\{p,f,\ldots\};N-1\rangle = [(E\underline{1}-\underline{H})^{-1}]_{0,-1}$$

and

$$\langle\{s,d,\ldots\};N\,|\,(E\underline{1}-\underline{H})^{-1}\,|\,\{p,f,\ldots\};N+1\rangle = [(E\underline{1}-\underline{H})^{-1}]_{0,1}$$

are, respectively, the coefficients of $\underline{Y}_{-1}$ and $\underline{Y}_{+1}$ in the expression Eq. (5.8) for $\underline{X}_0$. One has

$$[(E\underline{1}-\underline{H})^{-1}1]_{0,1} = -[(E\underline{1}-\underline{H})^{-1}]_{0,0}(E\underline{1}-\underline{H})_{0,1} \times\{[(E\underline{1}-\underline{H})_{1,1}]^{-1}\}_{1,1}\,, \tag{5.17a}$$

$$[(E\underline{1}-\underline{H})^{-1}]_{0,-1} = -[(E\underline{1}-\underline{H})^{-1}]_{0,0}(E\underline{1}-\underline{H})_{0,-1} \times\{[(E\underline{1}-\underline{H})_{-1,-1}]^{-1}\}_{-1,-1}\,. \tag{5.17b}$$

An important characteristic of these expressions is that nondiagonal block matrices of the inverse matrix are given in terms of the diagonal ones. Thus the calculation is reduced to that of the already-defined diagonal elements, Eqs. (5.9) and (5.15). Again the connection with Yeh and Stehle's 1977 results[1] is achieved by making the above-mentioned substitutions $[(E\underline{1}-\underline{H})^{-1}1]_{0,0} = G_N$, $(E\underline{1}-\underline{H})_{0,\pm1} = P_N V P_{N\pm1}$; $[(E\underline{1}-\underline{H})_{M,M}]^{-1} = G_{N+M}$, etc., which permit us to recover their Eq. (3.29).

Generalization to the case of higher-order transitions may be made in a similar way by suitably increasing the number of block matrices included in the partitioning of $(E\underline{1}-\underline{H})$. For instance, the expression of a general M-photon transition amplitude $\langle a;N\,|\,(E\underline{1}-\underline{H})^{-1}\,|\,b;N+M\rangle = [(E\underline{1}-\underline{H})^{-1}]_{0,M}$ reads

$$[(E\underline{1}-\underline{H})^{-1}]_{0,M} = [(E\underline{1}-\underline{H})^{-1}]_{0,0}[V_{0,1}][(E\underline{1}-\underline{H})_{1,1}]^{-1}[V_{1,2}][(E\underline{1}-\underline{H})_{2,2}]^{-1}[V_{2,3}]\cdots[V_{M-2,M-1}] \times[(E\underline{1}-\underline{H})_{M-1,M-1}]^{-1}[V_{M-1,M}][(E\underline{1}-\underline{H})_{M,M}]^{-1}\,, \tag{5.18}$$

where $[(E\underline{1}-\underline{H})^{-1}]_{0,0}$ is given in Eq. (5.9). As before the nondiagonal block matrices $[V_{J,J+1}]$, when entering in a matrix product, play the role of projectors onto given subspaces. It follows that, as shown in Sec. V A we need only determine the leading block element of the inverse $[(E\underline{1}-\underline{H})_{J,J}]^{-1}$. These elements exhibit the continued-fraction structure given in the expression Eq. (5.15). Equation (5.18) correspond to the amplitude entering Eq. (3.37) of Gontier, Rahman, and Trahin's paper[1] and to Eq. (3.28) of Yeh and Stehle's 1977 paper.[1]

C. Perturbation theory and eigenvalues of the block truncated Floquet Hamiltonian

Either by power series expanding the denominator of Eqs. (5.9) using Eq. (5.15) or by direct partitioning of the Floquet matrix, Eq. (3.5) itself, it is straightforward to write perturbation expansions of the Brillouin-Wigner type for the dressed or Floquet energies, thus making explicit the relationship of truncations of the Floquet Hamiltonian and either usual or continued-fraction perturbative techniques. As usual, it is convenient to introduce diagrammatic representations for the resulting expansions, as within the framework of the diagrams the origin of the large numbers of higher-order terms in the expansion becomes clear. Figure 10 indicates the structural framework of allowed diagrams through eighth order in perturbation theory using a notation similar to that of Yeh and Stehle,[1] indicating both the number of *interactions* (or "order" in the expansion, denoted by k) and the extent of the *walks* in photon number away from the reference photon number N. Rules for construction of individual diagrams and their evaluation are straightforward. (1) An individual diagram (for the linear polarization case at hand) is constructed by beginning at the node 0 and moving, following the arrows, successively to nodes $1,2,\ldots,k$. For a contribution to the kth-order correction to the dressed state $\epsilon_{nl}+N\omega$ the path must end at the kth step with a node at photon number N. The topologically distinct paths corre-

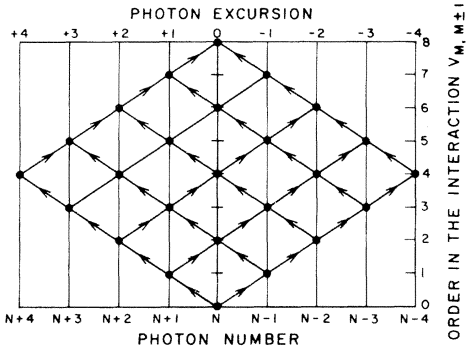

FIG. 10. Skeleton form indicating the possible types of diagrams contributing to a dressed-state energy. Order with respect to the interaction is plotted up the vertical axis. For each change in order the photon number must change by ±1. Assuming N to be the reference photon number all diagrams of order k are obtained by considering all distinct paths connecting the node at photon number N, order 0, to photon number N, order k, following the arrows in the indicated directions. See Fig. 11 for examples. It may be shown that the total number of paths for such a $k=2J$ order diagram is $\binom{2J}{J}$. As will be seen, truncation of the Floquet expansion, at a finite number of Floquet blocks, corresponds to truncation to a maximum excursion J in photon number, but is infinite order in the interaction. Rules for construction and evaluation of the diagrams are given in the text.

spond in a one-to-one way to individual contributions to the perturbation expansion, all diagrams are weighted equally, and all must be included. For example, the specific paths in second and fourth order are displayed in Figs. 11(a) and 11(b) as are a few of the sixth-order paths in Fig. 11(c). (2) Diagrams are evaluated in terms of the unperturbed propagators, and dipoled interaction term. The first and last nodes give the diagonal matrix element of the unperturbed states whose dressed energy is desired. Each directed arrow corresponds to a transition from M to $M\pm1$ photons and contributes a factor $V_{M,M\pm1}$. Each internal node (i.e., those with an arrow entering and leaving) contributes an unperturbed propagator $[E+N\omega-H^0(M)]^{-1}$ with M corresponding to the photon number of the given node.

Taking the $(1s+N\omega)$ state of atomic hydrogen as an example, we have

$$E=\epsilon_{1s}+N\omega \tag{5.19}$$

in zeroth order and

$$E=\epsilon_{1s}+N\omega+\left\langle 1s\left|V\frac{1}{E-H(N+1)}V\right|1s\right\rangle + \left\langle 1s\left|V\frac{1}{E-H(N-1)}V\right|1s\right\rangle \tag{5.20}$$

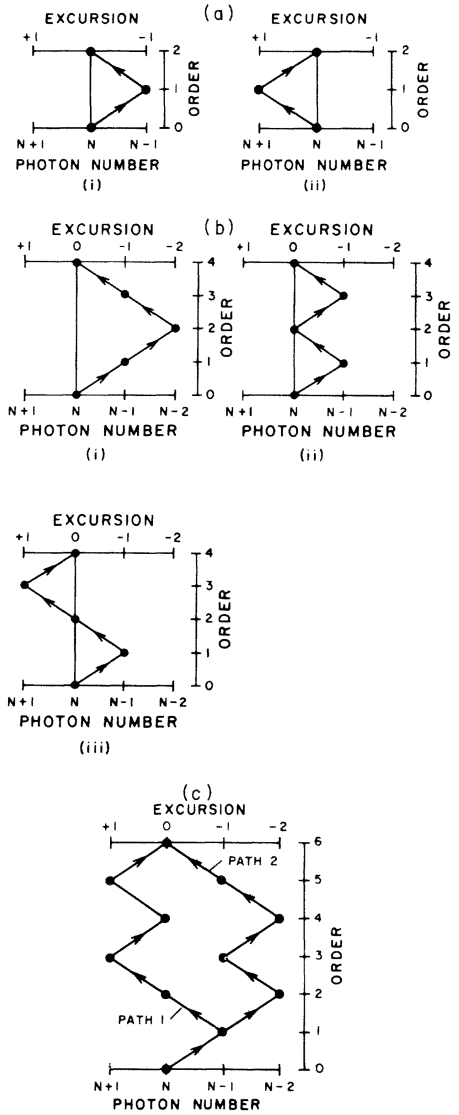

FIG. 11. (a) Paths giving rise to second-order contributions to the dressed energy. (i) corresponds to a virtual absorption, and (ii) to a virtual emission of a photon. Resulting second-order corrections to $(\epsilon_{1s}+N\omega)$ are shown in Eq. (5.1b). (b) Three paths giving rise to fourth-order contributions to the dressed energy. Three other paths, which are reflections of these through the vertical 0 excursion axis also contribute. (c) Two of the possible $\binom{6}{3}=20$ paths contributing to sixth-order contributions to the dressed-state energy. Diagram of path 2 is evaluated in the text.

in second order [corresponding to Fig. 11(a)].

A single sixth-order example should suffice to complete the discussion. The diagram in Fig. 11(c), is evaluated as path 2,

$$\left\langle 1s \left| V\frac{1}{E-[H^0(N-1)]}V\frac{1}{E-[H^0(N-2)]}V\frac{1}{E-[H^0(N-1)]}V\frac{1}{E-[H^0(N-2)]}V\frac{1}{E-[H^0(N-1)]}V \right| 1s \right\rangle . \tag{5.21}$$

We note that if intermediate states with N photons occur, the $1s$ state will be omitted in the spectral resolutions.

Within the framework of this simple diagrammatic notation, we can now make explicit the relationship between perturbation theory for an individual eigenvalue and truncation of the Floquet Hamiltonian, which will be necessary in any numerical approximation scheme. Figure 12 shows the skeleton diagrams contributing to the dressed-state energies corresponding to various truncations of the Floquet Hamiltonian. It is seen that each level of truncation corresponds to infinite-order perturbation theory, measured in terms of the number of interactions with the field, and that convergence in terms of inclusion of a sufficient number of Floquet block matrices is convergence with respect to the maximum (and/or minimum) excursion in photon number.

For completeness we briefly indicate the structure of the Rayleigh-Schrödinger expansion for the dressed-state energies. The symbolic diagrammatic expansion of Figs. 11 and 12 is simple because it is a Brillouin-Wigner expansion. That is, the sought after dressed-state energy appears on both sides of the expansion: It appears alone on the left-hand side of the expansion as the desired result, and on the right-hand side in all of the denominators. A Goldstone-type diagrammatic expansion representing the Rayleigh-Schrödinger perturbation expansion of the dressed-state energy follows from successive formal iteration of the Brillouin-Wigner expansion,[34] to successively remove the unknown energy to higher and higher order, followed by successive reexpansion, until all of the denominators are of the form $[\epsilon_{1s}+N\omega-(H_I^0\pm M\omega)]^{-1}$. This iterative process, which has been exhaustively discussed in the many-body context by Brandow,[34] Brueckner,[35] and others, gives rise to a much more complex perturbation expansion, explaining the difficulties which arise when the reverse process is attempted, and making the advantages of the partitioning technique especially clear. The imaginary part of the Rayleigh-Schrödinger-type perturbation expansion for E_{1s} will yield, order by order, the usual (for example, see Refs. 15 and 36) perturbation contributions to one-, and two-, and three-photon ionization, etc., provided that the correct limit as ϵ_{1s} approaches the real axis is taken. This is easily verified by direct introduction of the diagonal atomic spectral representations of $[\epsilon_{1s}+N\omega-(H_I^0\pm M\omega)]^{-1}$.

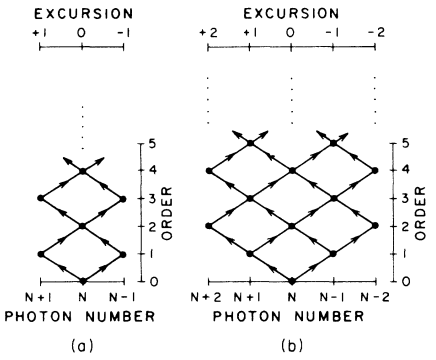

FIG. 12. Skeleton diagrams corresponding to various block truncations of the Floquet matrix. Truncation in the number of Floquet blocks to those containing N, and $N\pm1$ photons (i.e., to three blocks) gives rise to the skeleton of Fig. 4(a), which shows that a truncation in the photon excursion, but *not* perturbation order is implied. Figure 4(b) shows the skeleton for contribution to the dressed energies obtained by truncation of the Floquet Hamiltonian to five blocks, and to excursions of $0, \pm1, \pm2$ photons about the reference number.

VI. CALCULATION OF ADIABATIC MULTIPHOTON IONIZATION RATES

As demonstrated in Sec. IV, the truncated time-independent Floquet Hamiltonian $H_\omega(\theta)$ has complex eigenvalues and eigenvectors which are easily obtained computationally and which we expect to be related to time dependences of multiphoton ionization processes. A general discussion of this relationship appears in the following paper HRR. What is discussed here is the possibility of relating individual complex eigenvalues of $H_\omega^{\mathcal{F}}(\theta)$ to ionization rates. This will be the case only when the eigenvalue of interest is isolated, namely, when it is possible to prepare adiabatically the dressed state under consideration. This simple fact follows immediately from the discussion of time evolution in Sec. VI A. Section VI B contains illustrations of the utility of the method in intense-field, one- and two-photon ionization of hydrogen, using complex eigenvalues calculated by the methods of Sec. IV.

A. Time dependence and dilatation transformation

In the Floquet representation, the time dependence of an initial direct-product state

$|\alpha\rangle = |\alpha(0)\rangle$ is given by

$$|\alpha(t)\rangle = e^{-iH_\omega^{\mathcal{I}} t}|\alpha\rangle \tag{6.1}$$

and the bound-bound transition probability given as

$$P_{\alpha\to\beta}(t) = |\langle\beta|e^{-iH_\omega^{\mathcal{I}} t}|\alpha\rangle|^2 , \tag{6.2}$$

where Eq. (6.2) assumes an average over the initial phase of the monochromatic laser of frequency ω.[20]

For computational purposes, we write $e^{-iH_\omega^{\mathcal{I}} t}$ in terms of the integral representation

$$\langle\beta|e^{-iH_\omega^{\mathcal{I}} t}|\alpha\rangle = \left\langle\beta\left|\frac{1}{2\pi i}\int_{\mathscr{C}}\frac{e^{-izt}}{z-H_\omega^{\mathcal{I}}}dz\right|\alpha\right\rangle , \tag{6.3}$$

where $\mathscr{C}$ is any contour enclosing the spectrum of $H_\omega^{\mathcal{I}}$ in a positive sense, as shown in Fig. 7. As in Sec. II B, the dilatation transformation $H_\omega^{\mathcal{I}} \to H_\omega^{\mathcal{I}}(\theta)$ provides the new integral representation

$$\langle\beta|e^{-H_\omega^{\mathcal{I}} t}|\alpha\rangle = \left\langle\beta(\theta)\left|\frac{1}{2\pi i}\int_{\mathscr{C}}\frac{e^{-izt}}{z-H_\omega^{\mathcal{I}}(\theta)}dz\right|\alpha(\theta)\right\rangle , \tag{6.4}$$

where, as the spectrum of $H_\omega^{\mathcal{I}}(\theta)$ differs considerably from that of $H_\omega^{\mathcal{I}}$, the contour may be deformed advantageously just as shown in Fig. 3 in the dc case.[37] If an adiabatically prepared dressed state $|\alpha(\theta)\rangle$, which is an eigenfunction of $H_\omega^{\mathcal{I}}(\theta)$ is propagated via Eq. (6.4) only a single term survives the contour integration, and the time evolution is pure exponential.

In actual calculations, as discussed in Sec. IV, $H_\omega^{\mathcal{I}}(\theta)$ is projected onto a discretized atomic spectrum, and takes on the block-matrix structure shown in Fig. 6. This implies the matrix spectral resolution

$$\frac{1}{z-\bar{H}_\omega^{\mathcal{I}}(\theta)} = \sum_i |\tilde{i}\rangle\frac{1}{z-\tilde{E}_i}\langle\tilde{i}| , \tag{6.5}$$

where the $|\tilde{i}\rangle$ and $\langle\tilde{i}|$ being right and left eigenvectors of the complex symmetric matrix $\bar{H}_\omega^{\mathcal{I}}(\theta)$, i.e.,

$$\bar{H}_\omega^{\mathcal{I}}(\theta)|\tilde{i}\rangle = \tilde{E}_i|\tilde{i}\rangle \tag{6.6a}$$

and

$$\langle\tilde{i}|\bar{H}_\omega^{\mathcal{I}}(\theta) = \langle\tilde{i}|\tilde{E}_i \tag{6.6b}$$

$|\tilde{i}\rangle$ and $\langle\tilde{i}|$ form a bi-orthogonal set

$$\langle\tilde{i}|\tilde{j}\rangle = \delta_{ij} . \tag{6.6c}$$

Owing to the symmetry of $\bar{H}_\omega^{\mathcal{I}}(\theta)$, we have $\langle\tilde{i}| = (|\tilde{i}\rangle)^T$ rather than $\langle\tilde{i}| = (|\tilde{i}\rangle)^\dagger = [(|\tilde{i}\rangle)^T]^*$. Here T is the transpose, and the asterisk is the complex-conjugation operation; thus the dagger is the usual Hermitian conjugate. We consider two examples.

B. Adiabatic one-photon-dominated ionization

In the frequency region $\omega > 0.5$ a.u. the direct one-photon ionization channel is open for ground-state atomic H:

$$\omega + \mathrm{H}(1s) \to \mathrm{H}^+ + e^- . \tag{6.7}$$

In this case the complex eigenvalue $\tilde{E}_{1s}(\omega)$ is isolated, and represents the complex dressed energy of the state obtained adiabatically from the field-free $1s$ hydrogenic state. Assuming an atom prepared in this adiabatic state [only one term contributes to the expansion of Eq. (6.5)], we can ask for the field and frequency dependence of the ionization rate in terms of an intensity-dependent cross section (i.e., the rate divided by I) intensity normalized to the expected one-photon-dominated processes. The cross section, obtained directly from $\mathrm{Im}[\tilde{E}_{1s}(\omega)]/I$ is shown in Table I. At low fields ($F \lesssim 0.01$ a.u.) the eigenstate $|\tilde{1s}\rangle$ is essentially the (analytically continued) $1s$ state, and, as expected, gives an intensity-independent photoabsorption cross section identical to the usual photoeffect cross section calculated using the exact hydrogenic $1s$ ground and p-wave continuum states, with the assumption of the dipole approximation. At higher fields we might expect that the cross section will increase as direct many-photon ionization processes add to the ionization flux.[38,39] It is evident, from the cross sections of Table V that for frequencies near threshold there is a fairly substantial high field enhancement of the usual one-photon cross section. This enhancement dies off very quickly at higher frequencies. This is presumably due to the fact that two-photon processes are in one-photon resonance with the usual p-wave continuum, which has a substantial oscillator strength near threshold, but which decays quite rapidly as a function of frequency. Table VI gives a feeling for the complexity of the situation as the external rms field becomes an appreciable fraction of the internal atomic field strength, 20% in this case. The decomposition over unperturbed direct product states shows that, although the adiabatically prepared state is dominantly $1s$, other states (dominated by $|2p;N-1\rangle$) are beginning to play a substantial role. This implies a difference in time evolution of the bare $1s$ state with respect to sudden or adiabatic field turn-on of the external field. Adiabatic turn-on would result in the ionization generalized cross

TABLE V. Intensity-dependent one-photon dominated ionization cross section $\sigma_1(a_0^2)$ at rms field $F_{\rm rms}$ for atomic hydrogen in the state adiabatically prepared from $1s$ ground state. Generalized cross section σ_1 is defined proprotional to $\tilde{\Gamma}_{1s}/I$ where $\tilde{\Gamma}_{1s}$ is the width of the complex dressed $1s$ state, and $I=F_{\rm rms}^2$, the rms field intensity. For $F_{\rm rms}\lesssim 10^{-2}$ a.u., σ_1 is field independent to high accuracy and equal to the usual photoeffect cross section. As the rms field strength is increased the cross section is seen to be enhanced, presumably by direct two-, three-, . . . photon ionization processes (Refs. 38 and 39). In the high-field cases details of state preparation will be important, and these adiabatic cross sections are difficult to observe.

	$F_{\rm rms}$ (a.u.)						
ω	10^{-4} [a]	10^{-2} [a]	0.0025[b]	0.05[b]	0.10[c]	0.15[c]	0.20[c]
0.50	0.225	0.225	0.226	0.228	0.237	0.242	0.253
0.55	0.174	0.174	0.175	0.176	0.179	0.183	0.186
0.60	0.138	0.138	0.138	0.138	0.140	0.142	0.142
0.80	0.062	0.062	0.062	0.062	0.062	0.062	0.062
1.00	0.033	0.033	0.033	0.033	0.033	0.033	0.033

[a]For these field strengths three Floquet blocks (A and $A\pm 2\omega$) were used with the A's defined by use of $15s, 15p, 15d$ atomic functions with $\lambda=1.2$, and $\theta=0.45$ rad.

[b]For these field strengths the atomic basis was extended to include $15f$ functions and the $(A-4\omega)$ Floquet block added to the three Floquet blocks of a. Again $\lambda=1.2$ and $\theta-0.45$ rad.

[c]Atomic basis of b was augmented with 15 "g" functions and the Floquet block $(A+4\omega)$ added to the four Floquet blocks of b, above. Again $\lambda=1.2$ and $\theta=0.45$ rad.

section of Table V. Sudden turn-on would give rise to substantial transients due to non-negligible projections onto many dressed states, as implied by the projections of Table II. Again, such more complex time dependences are the subject of HRR. However, even without this latter analysis it is evident that the inclusion of resonant free-free multiphoton transitions is of no great difficulty in the present matrix Floquet method. This is because the complex rotation of coordinates has moved all of the continua away from the real axis avoiding any need for careful evaluation of the principal-value integrals which would arise in the usual formulation of continued-fraction perturbation theory.

TABLE VI. Projection of the dressed $1s$ state of atomic hydrogen with $E_{1s}=-0.423\,305-i0.051\,543$ at $F_{\rm rms}=0.2$ (a.u.) and $\omega=0.6$ (a.u.) onto the unperturbed dressed states $|nl;N\pm M\rangle$. Matrix Floquet calculation for these intensity and field parameters is that discussed in Table V. Projections shown are the complex numbers $\langle\tilde{E}_{1s}|nl;N-M\rangle$ for $M=0,1,2$. Notation angular brackets denote a real scalar product as discussed in Sec. VI. It is evident that at this high field substantial mixing of atomic states has taken place.

Unperturbed dressed state $\lvert nl;M\rangle$	Vector projections (real scalar product) $\langle\tilde{E}_{1s}(F=0.2,\omega=0.6)\lvert nl;N-M\rangle$
$\lvert 1s;0\rangle$	$0.7069+i0.2729$
$\lvert 2s;0\rangle$	$-0.055+i0.012$
$\lvert 3s;0\rangle$	$-0.023+i0.020$
$\lvert 2p;-1\rangle$	$0.2232-i0.054$
$\lvert 3p;-1\rangle$	$0.046-i0.050$
$\lvert 4p;-1\rangle$	$0.013-i0.007$
$\lvert 2s;-2\rangle$	$0.0042-i0.0044$
$\lvert 3s;-2\rangle$	$-0.0059+i0.011$
$\lvert 3d;-2\rangle$	$-0.0052+i0.002$

C. Adiabatic two-photon-dominated ionization

In the frequency regime near $\omega=0.375$ a.u. the $1s\rightarrow(2p\text{-}\omega)$ transition is in near-resonance and the ionization process is dominated by two-photon ionization. The fact that the unperturbed $|1s;N\rangle$, and $|2p;N-1\rangle$ states become degenerate implies that the corresponding complex Floquet eigenvalues will be nearly degenerate, and an avoided crossing will occur as ω is swept through resonance. This is illustrated in Fig. 10, where the real parts of the complex dressed energies are indeed seen to undergo such an avoided crossing. (More detailed discussion of such complex avoided crossings appears in HRR.) The nearest approach of the eigenvalues is a strong function of field strength and is a measure of the $1s\rightarrow 2p$ Rabi frequency. Discussion of the time dependence of the resonant and near-resonant ionization process appears in HRR. In the remainder of this section we discuss the information directly implied in the imaginary parts of the individual dressed states. Thus, we assume that we can experimentally prepare a pure dressed state at $t=0$, and also observe its

subsequent decay. This implies that information will not be obtained for near-resonant processes, as adiabatic field turn-on (at constant ω) is then not possible. Nearness to resonance is defined in terms of the Rabi splittings of Fig. 13, and thus for low fields adiabatic turn-on is a reasonable assumption except almost exactly on resonance. This is illustrated by the results of Table VII, where the generalized cross section $\tilde{\sigma}_2(\text{Floquet}) \equiv \tilde{\Gamma}_{1s}/I^2$ calculated from the eigenenergy $(\tilde{\epsilon}_{1s} - i\tilde{\Gamma}_{1s}/2)$ of the dressed state, which is dominantly $|1s;0\rangle$ rather than $|2p;-1\rangle$, is compared with the second-order perturbation calculations of Chan and Tang.[40] The agreement is seen to be excellent, neither method being valid on resonance. The intensity dependence of $\tilde{\sigma}_2$ (Floquet) is shown in Fig. 14, where the mismatches in the estimated cross sections at the $1s \rightarrow 2p$ and $1s \rightarrow 3p$ resonances give a measure of the failure of the adiabatic approach on resonance. It is interesting to note that at the highest field strength ($F_{\text{rms}} = 0.1$ a.u.) the adiabatic generalized cross section shows no resonant structure whatever, and that due to the enormous Rabi broadening (bound-bound power broadening) the off-resonant generalized cross section is beginning to decrease,

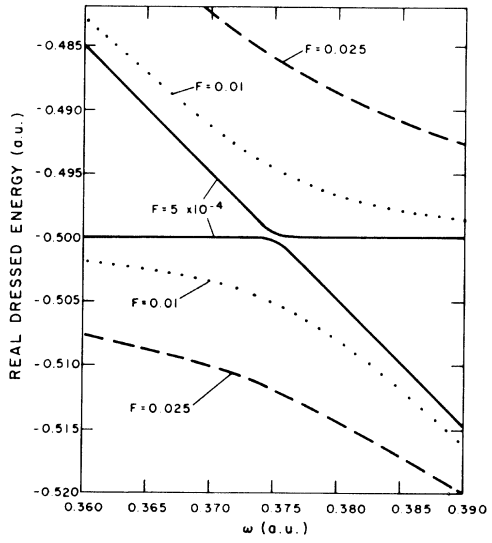

FIG. 13. Real parts of the dressed energies corresponding to the bare $|1s;0\rangle$ and $|2p;-1\rangle$ states near the $|1s;0\rangle$, $|2p;-1\rangle$ degeneracy at $\omega = 0.375$ a.u. Avoided crossings of the real parts of the complex Floquet eigenvalues are shown for three field strengths. Strong field dependence of this avoided crossing corresponds to the fact that it is Rabi, rather than ionization, broadening which causes quenching of the resonant enhancement of the ionization cross section near the $|2p;-1\rangle$ and $|3p;-1\rangle$ resonances. See HRR (Ref. 6).

TABLE VII. Generalized cross sections for two-photon ionization of the $1s$ state of hydrogen calculated for "low"-field strength ($F_{\text{rms}} = 5 \times 10^{-4}$ a.u.) from the dressed $1s$ complex Floquet eigenvalue (σ_2, Floquet). In the low-field limit it is seen that the Floquet calculations agree with second-order perturbation calculations of Chan and Tang (σ_2, PT), as is to be expected in this intensity region. Well away from resonance the results should be identical and thus provide a comparison of the numerical convergence of the discretization and of the iterative complex eigenvalue determination, with numerical methods of Ref. 40. Agreement is approximately one part in 10^3 off resonance.

Wavelength λ (Å)	Floquet[a] $\tilde{\sigma}_2$ (cm^4/W)	PT[b] $\tilde{\sigma}_2$ (cm^4/W)	Wavelength λ (Å)	Floquet[a] $\tilde{\sigma}_2$ (cm^4/W)	PT[b] $\tilde{\sigma}_2$ (cm^4/W)	Wavelength λ (Å)	Floquet[a] $\tilde{\sigma}_2$ (cm^4/W)	PT[b] $\tilde{\sigma}_2$ (cm^4/W)
1700	1.026(−32)	1.025(−32)	1200	6.373(−32)	6.303(−32)	1040	2.987(−33)	3.015(−33)
1600	9.165(−33)	9.154(−33)	1180	6.723(−33)	6.654(−33)	1035	5.358(−33)	5.450(−33)
1500	8.389(−33)	3.830(−33)	1160	1.426(−33)	1.413(−33)		$1s$-$3p$ resonance	
1450	8.251(−33)	8.243(−33)	1140	4.445(−34)	4.415(−34)	1020	7.052(−33)	6.752(−33)
1400	8.457(−33)	8.450(−33)	1130	3.272(−34)	3.256(−34)	1010	3.566(−34)	3.456(−34)
1350	9.417(−33)	9.413(−33)	1120	3.049(−34)	3.042(−34)	1005	1.932(−34)	1.870(−34)
1300	1.276(−32)	1.276(−32)	1110	3.357(−34)	3.359(−34)	1000	1.927(−34)	1.892(−34)
1250	3.448(−32)	3.467(−32)	1100	4.013(−34)	4.013(−34)	995	2.601(−34)	2.564(−34)
1240	5.613(−32)	5.671(−32)	1080	6.163(−34)	6.174(−34)	990	3.808(−34)	3.772(−34)
	$1s$-$2p$ resonance		1060	1.052(−33)	1.055(−33)	980	1.148(−33)	1.149(−33)

[a]In the Floquet calculations $F_{\text{rms}} = 5 \times 10^{-4}$, $\lambda = 1.2$ and $\theta = 0.45$ rad, $25s, 25p, 25d$ atomic functions, and three Floquet blocks, $\underline{A}$, $A \pm 2\omega$ were used.
[b]Perturbative calculations of Chan and Tang (Ref. 40).

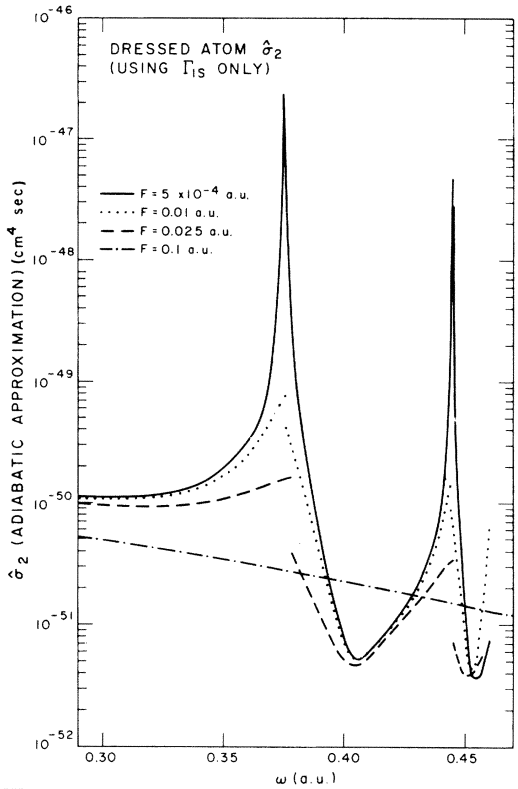

FIG. 14. Adiabatic generalized cross section $\sigma_2 \sim \tilde{\Gamma}_{1s}/I^2$, for the two-photon-dominated ionization of the $1s$ state of atomic hydrogen near the $2p$ and $3p$ intermediate one-photon resonances. These approximate cross sections were calculated assuming that the adiabatically prepared complex dressed $1s$ state decays exponentially with lifetime $\tilde{\Gamma}_{1s}^{-1}$ [i.e., $\mathrm{Im}(E_{1s}) = -\tilde{\Gamma}_{1s}/2$], a quite reasonable approximation off resonance. At low fields [$F_{\mathrm{rms}} \leq \sim 10^{-3}$ a.u. $\sim 10^{10}$ W/cm^2 (rms)] this approximation gives σ_2 in numerical agreement with that obtained by the usual second-order perturbation theoretic formulation, except on resonance where both of these simplistic formulations break down: Second-order perturbation theory, of course, diverges on resonance as the avoided crossings of Fig. 13 are ignored (i.e., Rabi broadening is omitted); in the Floquet case the states in question cannot be adiabatically prepared starting at the exact resonance frequency. Rabi broadening has completely quenched the resonant enhancement at $F = 0.1$ a.u. [$\sim 3.5 \times 10^{14}$ W/cm^2 (rms)]. This same conclusion follows from the more complete analysis of HRR (Ref. 6).

implying that the rate is no longer scaling as I^2, due to saturation.

It is clear that a great deal of information is contained in the imaginary parts of the complex Floquet eigenvalues; however, a more serious discussion of multiphoton ionization-rate processes requires more detailed discussion of time dependences, including the laser turn-on. These topics are the subjects of HRR.

VII. DISCUSSION

In this paper the following has been accomplished: Floquet theory has been generalized to include the presence of multiple ionization continuua in such a manner as to make connection with more usual perturbative approaches. Introduction of an appropriate analytic continuation of the generalized Floquet Hamiltonian alters the spectrum in such a way as to allow direct calculation of the complex dressed states which represent the (decaying) states of the atom plus laser field. It has been shown that such complex eigenvalues may be systematically obtained using L^2 basis-set expansions, thus taking advantage of the fact that the eigenfunctions of $H_\omega^{\mathcal{F}}(\theta)$ are L^2 in the rotated coordinates. In this paper the imaginary parts of the complex eigenvalues are shown to contain substantial physical information. In HRR it is shown how this information may be used to directly calculate the time evolution of the atom plus field system, in addition to the adiabatic generalized cross sections reported here.

ACKNOWLEDGMENTS

This work was supported in part by National Science Foundation Grants Nos. CHE-77-16307, CHE-80-11412, PHY-76-04761, and PHY-79-04928. A. M. has been supported in part by grants from the North Atlantic Treaty Organization. W. P. R. acknowledges Fellowship support during earlier stages of this work from the J. S. Guggenheim Memorial Foundation, and from the Council on Research and Creative Work of the University of Colorado. A. M. gratefully acknowledges the hospitality of the staff of the Joint Institute for Laboratory Astrophysics during a visit in 1979. The authors gratefully acknowledge the computational advice and assistance of Chela V. Kunasz and Linda Kaufman.

APPENDIX: NUMERICAL ESTIMATES OF INDIVIDUAL COMPLEX EIGENVALUES

1. Inverse iteration

If only a small number of eigenvalues and eigenvector of a matrix $\underline{A}$ are needed, inverse iteration[28] is very convenient. Given an estimate of a (complex eigenvalue σ near an eigenvalue a) successive solution of the linear equation

$$(\underline{A} - \sigma \underline{\mathbb{1}})\underline{x}_n = \underline{x}_{n-1} \quad n = 1,2,3,\ldots \tag{A1}$$

effectively constructs $\underline{y}_n = [(\underline{A} - \sigma \underline{\mathbb{1}})^{-1}]^n \underline{x}_0$, where $\underline{x}_0$ is an arbitrary initial vector. As long as $\underline{x}_0$ is not exactly orthogonal to the eigenvector

$\underline{c}_i(\underline{A}\,\underline{c}_i = a_i\underline{c}_i)$, and as long as σ is closer to a_i than to any other eigenvalue

$$\underline{y}_n \approx \frac{1}{(a_i-\sigma)^n}\underline{c}_i \tag{A2}$$

to within normalization, allowing calculation of both a_i and $\underline{c}_i$, given an initial guess. This has proved to be a highly advantageous method of finding complex eigenvalues and vectors. Choice of σ and $\underline{x}_0$ has never been difficult and the choice $\underline{x}_0=(1,1,1,1,\ldots)$ followed by normalization has proved adequate in all cases investigated.

2. Solution of block tridiagonal equations

Implementation of inverse iteration requires solution of the linear system

$$[\underline{H}_\omega^{\mathcal{F}}(\theta)-\sigma\underline{1}]\underline{x}=\underline{f}\ , \tag{A3}$$

where $\underline{H}_\omega^{\mathcal{F}}(\theta)$ is the matrix Floquet Hamiltonian; $\underline{1}$ is the identity and $\underline{f}$ is a known vector. The matrix $[\underline{H}_\omega^{\mathcal{F}}(\theta)-\sigma\underline{1}]$ has block tridiagonal structure

$$\begin{pmatrix} \underline{A}_1 & \underline{B}^T & \underline{0} & \underline{0} \\ \underline{B} & \underline{A}_2 & \underline{B}^T & \underline{0} \\ \underline{0} & \underline{B} & \underline{A}_3 & \underline{B}^T \\ \underline{0} & \underline{0} & \underline{B} & \ddots \end{pmatrix} \tag{A4}$$

which can be factored into upper ($\underline{U}$) and lower ($\underline{L}$) block matrices of the form[28]

$$\underline{L}=\begin{pmatrix} \underline{a}_1 & \underline{0} & \underline{0} & \cdots \\ \underline{B} & \underline{a}_2 & \underline{0} & \\ \underline{0} & \underline{B} & \underline{a}_3 & \\ & & & \ddots \\ 0 & & \underline{B} & \underline{a}_i \end{pmatrix}, \tag{A5a}$$

$$\underline{U}=\begin{pmatrix} \underline{1}_1 & \underline{\Gamma}_1 & & 0 \\ & \underline{1}_2 & \underline{\Gamma}_2 & \\ & & \underline{1}_3 & \underline{\Gamma}_3 \\ 0 & & & \ddots \end{pmatrix}, \tag{A5b}$$

where

$$\underline{a}_1=\underline{A}_1\ , \tag{A6a}$$

$$\underline{\Gamma}_1=(\underline{a}_1)^{-1}\underline{B}^T,\ \ldots\ , \tag{A6b}$$

$$\underline{\Gamma}_i=(\underline{a}_i)^{-1}\underline{B}^T\ , \tag{A6c}$$

where

$$\underline{a}_i=\underline{A}_i-\underline{B}\underline{\Gamma}_{i-1},\quad i=2,3,\ldots\ . \tag{A6d}$$

The decompostion allows solution of the linear system (A3) in a sequence of elementary steps each of which scales as n^3 being the dimension of the Floquet block $\underline{A}$. The solution $\underline{A}\underline{x}=\underline{f}$ where $\underline{A}=\underline{L}\underline{U}$ proceeds as $\underline{L}\underline{g}=\underline{f}$ and $\underline{U}\underline{x}=\underline{g}$. The first of these equations is solved sequentially with no need for storage of the $\underline{a}_i$'s; the $\underline{\Gamma}_i$'s needed for solution of $\underline{U}\,\underline{x}=\underline{g}$ are stored (out of core if need be) sequentially as computed. Matrix inversions are unnecessary as the $(\underline{a}_i)^{-1}\underline{B}^T$ are calculated by solution of linear equations. Thus, a Floquet Hamiltonian with $N_{\mathcal{F}}$ Floquet block-matrix solution of the eigensystem proceeds in $\sim N_{\mathcal{F}}n^3$ steps, n being the dimension of a single block. The fact that all of the $\underline{B}$'s are identical, and that $\underline{A}_1,\underline{A}_2,\underline{A}_3,\ldots$ only differ by addition of constant diagonal terms in addition to being block tridiagonal themselves results in minimal storage requirements. Taking full advantage of the block-matrix structure of the $\underline{A}$'s themselves reduces the number of operations needed for solution of the linear system to $\sim N_{\mathcal{F}}N_B m^3$ where $N_{\mathcal{F}}$ is the number of Floquet blocks, N_B the number of atomic symmetries in each Floquet block, and m is the number of L^2 basis functions needed to describe the bound and continuous spectra of a given atomic symmetry. This latter is typically 10 to 15 (see Figs. 7–9). Thus, for calculations with $N=3$, $N_B=3$, and $m=10$ (see Fig. 8) the order of $(3)^2(10)^3\approx 10^4$ operations (per iteration) are required. If advantage were not taken of the block-matrix structure the computation would require $(3\times 3\times 10)^3\sim 10^6$ operations, a considerable difference. Note that it is only the ratio of these numbers which is of significance as all housekeeping constants have been omitted. In the algorithms used here, full advantage of the complex symmetry has been taken, and a stabilized $\underline{L}\,\underline{U}$ decomposition code written by Dr. Linda Kaufman utilized.

---

*Permanent address: Laboratoire de Chime Physique (Laboratoire associé au Centre National de la Recherche Scientifique) Université Pierre et Marie Curie, 11 rue Pierre et Marie Curie, F-75231 Paris Cedex 05, France.

†Permanent address: Department of Chemistry, University of Kansas, Lawrence, Kansas 66045.

[1]For example, Y. Gontier, N. K. Rahman, and M. Trahin, Phys. Rev. A 14, 2109 (1976); Y. Gontier and M. Trahin, *ibid.* 19, 204 (1979); S. Yeh and P. Stehle, *ibid.* 15, 213 (1977); S. Swain, J. Phys. A 8, 1477 (1975); L. Mower, Phys. Rev. 142, 799 (1966); Phys. Rev. A 22, 882 (1980); S. Yeh and P. Stehle, J. Phys. B 14, 1741 (1981); R. I. Jackson and S. Swain, J. Phys. A 14, 3169 (1981).

[2]Brief presentations of these ideas appear in S.-I Chu and W. P. Reinhardt, Phys. Rev. Lett. 39, 1195 (1977) and in *Multiphoton Processes,* edited by J. Eberly and P. Lambropoulos (Wiley, New York, 1978), p. 171; S.-I Chu, Chem. Phys. Lett. 54, 367 (1978); C. Cerjan, R. Hedges, C. Holt, W. P. Reinhardt, K. Scheibner, and J. J. Wendoloski, Int. J. Quantum Chem. 14, 393 (1978); W. P. Reinhardt, in *Electronic and Atomic Collisions,* Invited Papers and Progress Reports of the International Conference on the Physics of Electronic and Atomic Collisions, XI edited by N. Oda and K. Takayanagi (North-Holland, Amsterdam, 1980), p. 729.

[3]The use of L^2 discretization (i.e., use of a finite subset of a complete, discrete atomic basis) to describe continuum processes is a well-established technique in single-photon ionization. See, H. A. Yamani and W. P. Reinhardt, Phys. Rev. A 12, 1222 (1975) for a detailed and explicit discussion of how the finite L^2 Laguerre-type basis used in the present paper discretizes a single-photon photoionization continuum, yet allows arbitrarily accurate photoionization cross sections to be determined. For further discussion, see W. P. Reinhardt, Comp. Phys. Commun. 17, 1 (1979); S. V. ONeil and W. P. Reinhardt, J. Chem. Phys. 69, 2126 (1978), and references therein; P. W. Langhoff, J. Sims and C. T. Corcoran, Phys. Rev. A 10, 829 (1974); P. W. Langhoff and C. T. Corcoran, J. Chem. Phys. 61, 146 (1974).

[4]Reviews of the use of complex coordinates (dilatation analyticity) in atomic and molecular physics have recently appeared. W. P. Reinhardt, Annu. Rev. Phys. Chem. 33, 223 (1982); B. R. Junker, Adv. At. Mol. Phys. 18, 207 (1982).

[5]Complex-coordinate techniques have been used in the framework of single-photon ionization by calculation of the one-photon cross section in terms of the imaginary part of the frequency-dependent polarizability. See, T. N. Rescigno and V. McKoy, Phys. Rev. A 12, 522 (1975); C. V. Sukumar and K. C. Kulander, J. Phys. B 11, 4155 (1978).

[6]C. Holt, M. Raymer and W. P. Reinhardt, Phys. Rev. A 27, 2971 (1983), hereafter referred to as HRR.

[7]W. P. Reinhardt, Int. J. Quantum Chem. S10, 359 (1976) and C. Cerjan *et al.*, Ref. 2, above.

[8]W. P. Reinhardt, Int. J. Quantum Chem. 21, 133 (1982).

[9]L. Benassi and V. Grecchi, J. Phys. B 13, 911 (1980).

[10]S. C. Leasure, K. F. Milfeld, and R. E. Wyatt, J. Chem. Phys. 74, 6197 (1981); C. Leforestier and R. E. Wyatt, Phys. Rev. A 25, 1250 (1982); K. F. Milford and R. E. Wyatt, Phys. Rev. A 27, 72 (1983).

[11]H. A. Silverstone, Phys. Rev. A 18, 1853 (1978); H. J Silverstone, B. G. Adams, T. Cizek, and P. Otto, Phys. Rev. Lett. 43, 1498 (1979), and references therein.

[12]E. C. Titchmarsh, *Eigenfunction Expansions Associated with Second-Order Differential Equations,* (Oxford University Press, Oxford, 1958), Vol. 2. See Yajima, Ref. 37, for the analogous ac result.

[13]Preliminary theoretical results are discussed in C. Cerjan, W. P. Reinhardt, and A. Avron, J. Phys. B 11, L201 (1978) and in C. Cerjan *et al.*, Ref. 2. A subsequent complete discussion appears in I. Herbst, Commun. Math. Phys. 64, 279 (1979).

[14]M. I. Goldberger and K. M. Watson, *Collision Theory* (Wiley, New York, 1964), Chap. 8 give a good discussion of the use of this representation to describe nonstationary-state time evolution.

[15]The time evolution of Eq. (2.8) is used as the basis for formulating multiphoton perturbation theory by P. Lambropoulos, Adv. At. Mol. Phys. 12, 87 (1976).

[16]See, for example, B. Simon, Ann. Math. 97, 247 (1973), for a discussion of the unitary transformation $U(\theta)$ which introduces the scale transformation: We have for $\theta > 0$,

$$\langle \phi,(z-H)^{-1}\chi\rangle = \langle \phi, U^{-1}U(z-H)^{-1}U^{-1}U\chi\rangle$$
$$= \langle \phi(\theta),[z-H(\theta)]^{-1}\chi(\theta)\rangle$$

in the upper-half z plane. Thus, $\langle \phi(\theta),[z-H(\theta)]^{-1}\chi(\theta)\rangle$ provides the required analytic continuation of $\langle \phi,(z-H)^{-1}\chi\rangle$ into the lower-half z plane. See also the discussion of Ref. 4.

[17]H. A. Yamani and W. P. Reinhardt, Ref. 3.

[18]S. Geltman, J. Phys. B 11, 3323 (1978).

[19]J. H. Shirley, Phys. Rev. 138, B979 (1965).

[20]See also the discussion of S. B. Barono, M. A. Narcowich, and F. J. Narcowich, Phys. Rev. A 15, 1109 (1977) for explicit discussion of Floquet perturbative techniques of use when the field-free operator has a continuous spectrum. See also Yajima, Ref. 37.

[21]S.-I Chu, Chem. Phys. Lett. 58, 462 (1978); 64, 178 (1979); S.-I Chu, J. Chem. Phys. 75, 2215 (1981).

[22]For example, Eq. (11) of Shirley, Ref. 19.

[23]Y. Gontier, N. K. Rahman and M. Trahin, Phys. Rev. A 24, 3102 (1981).

[24]M. Karplus and H. J. Kolker, J. Chem. Phys. 39, 1493 (1963).

[25]A. Dalgarno and J. T. Lewis, Proc. R. Soc. London, Ser. A 233, 70 (1955). The applications discussed in this paper, if applied independently to each atomic subblock of each Floquet block would amount to a linear variational implementation of the Dalgarno-Lewis technique at each level of a continued-fraction expansion. The method of Ref. 23 is, in this sense, implicit in the work of Ref. 2, above.

[26]P. O. Löwdin, in *Perturbation Theory and its Application to Quantum Mechanics,* edited by C. H. Wilcox (Wiley, New York, 1966), p. 225.

[27]Ben Noble, *Applied Linear Algebra* (Prentice-Hall, Englewood Cliffs, N.J., 1969), pp. 18–21.

[28]E. Isaacseon and H. B. Keller, *Analysis of Numerical Methods* (Wiley, New York, 1966), pp. 58–61.

[29]L. Rosenberg, Phys. Rev. A 14, 1137 (1976).

[30]H. S. Wall, *Analytic Theory of Continued Fractions* (Chelsen, New York, 1973).

[31]G. A. Baker, Jr., *Essentials of Padé Approximants* (Academic, New York, 1975), Chap. 21.

[32]The basic theory of matrix Padé approximants and continued fractions may be found in J. L. Basdevant, D. Bessis, and J. Zinn-Justin, Nuovo Cimento 60A, 185 (1969); J. Zinn-Justin, Phys. Rep. C 1, 55 (1971).

[33]A nonexhaustive list of recent applications of matrix Padé approximants to problems of physical interest is the following: A. Bambini, Phys. Rev. A 14, 1479 (1976); M. Allegrini, E. Arimondo, and A. Bambini, *ibid.* 15, 718 (1977); D. Bessis and G. Turchetti, Nucl. Phys. B123, 173 (1977); B. Bessis, P. Mery, and G. Turchetti, Phys. Rev. D 15, 2345 (1977); F. Ortolani and G. Turchetti, J. Phys. B 11, L207 (1978). See also, *Padé and Rational Approximation,* edited by E. B. Saff and R. S. Varga (Academic, New York, 1977) and references therein.

[34]B. Brandow, Rev. Mod. Phys. 39, 771 (1967).

[35]K. Brueckner, Phys. Rev. 100, 36 (1955).

[36]M. Göppert Mayer, Ann. Phys. (N.Y.) 9, 273 (1931).

[37]In the dc Stark problem the dilatation $r \rightarrow re^{i\theta}$ causes the continuous spectrum of the Coulomb Stark Hamiltonian to vanish identically, implying that $[z - H^{\text{Stark}}(\theta)]^{-1}$ is meromorphic in the finite complex z plane for any $\theta \neq 0$ (θ, real) (see Cerjan *et al.*, Ref. 2, and I. Herbst, Ref. 13). Figure 3 tacitly assumes that this is the case for the ac Stark problem—an unproven conjecture at this time. The fact that in the presence of an ac field there are no bound states, has recently been proven for all but a countable number of frequencies by K. Yajima, Commun. Math. Phys. 87, 331 (1982), following the earlier work of H. Kitada and K. Yajima, Duke Math J. 49, 341 (1982); J. S. Howland, Indiana Math J. 28, 471 (1979). However, in *either* the ac or dc case, an $N \times N$ matrix representational generally yields N complex eigenvectors and eigenvalues, and thus a residual "numerical" vestige of the continuous spectrum survives; see Cerjan *et al.*, Ref. 2. However, in cases except sudden turn-on, this residual vestige of the continuum has been empirically determined to play no role in determination of physically reasonable time dependences.

[38]Previous perturbative estimates of this effect have been made by W. Zernik and R. W. Klopfenstein, J. Math. Phys. 6, 262 (1965); S. Klarsfeld, Lett. Nuovo Cimento 3, 395 (1970); E. Karule, in *Multiphoton Processes,* edited by J. Eberly and P. Lambropoulos, Ref. 2; J. Phys. B 11, 441 (1978).

[39]Implicit in this conceptual model is the fact that photoelectrons will be produced at more than 1 kinetic energy: This has recently been observed in experiments on atomic xenon. See, P. Agostini, F. Fabre, G. Mainfray, G. Petite, and N. K. Rahman, Phys. Rev. Lett. 42, 1127 (1979).

[40]F. T. Chan and C. L. Tang, Phys. Rev. 185, 42 (1969).